Synthesis, UV-visible spectroelectrochemistry and theoretical characterization of new polypyridyl Ru(II) complexes containing 2, 4, 6 -tris(2-pyridyl)-1, 3, 5- triazine as precursors for water oxidation catalysts

Sofía E. Domínguez †, Faustino E. Morán Vieyra ††, Florencia Fagalde † *

† *INQUINOA (UNT-CONICET), Instituto de Química Física, Facultad de Bioquímica, Química y Farmacia, Universidad Nacional de Tucumán, Ayacucho 471, (T4000INI) San Miguel de Tucumán, Argentina.*
†† *INBIONATEC (UNSE-CONICET) Instituto de Bionanotecnología del NOA,, Universidad Nacional de Santiago del Estero, RN9, Km 1123, (G4206XCP) Santiago del Estero, Argentina.*
Corresponding Author e-mail: florencia.fagalde@fbqf.unt.edu.ar

Supporting Information

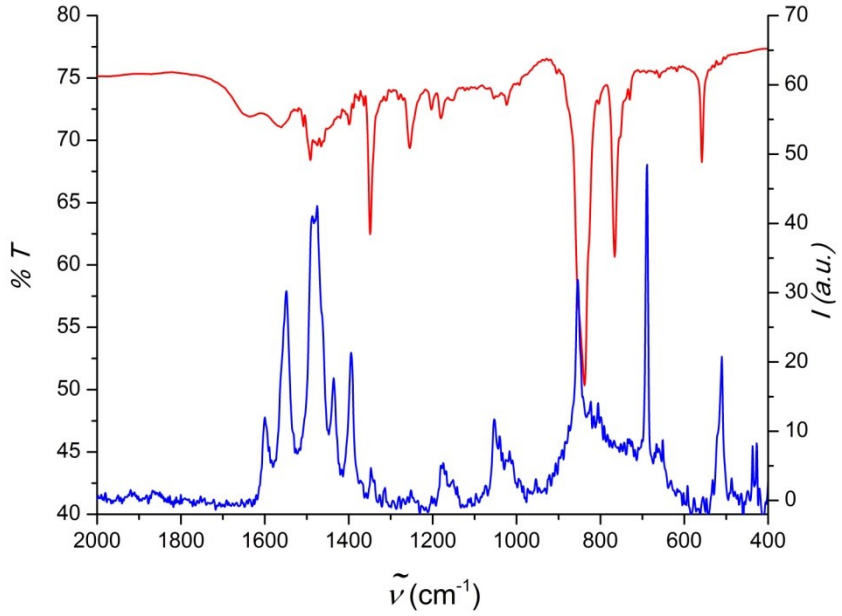

Figure S1. Infrared spectra as KBr pellets (left axis, red line) and Raman spectra (right axis, blue line) of complex **(1)**PF_6.

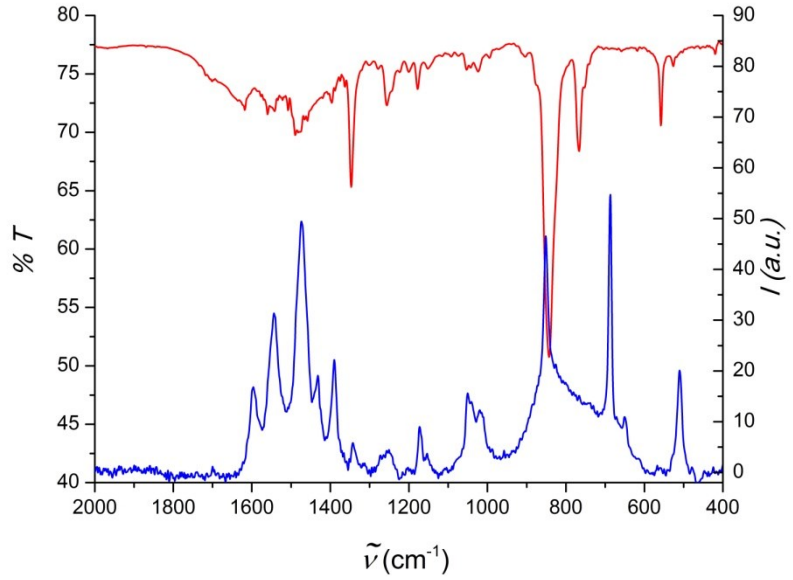

Figure S2. Infrared spectra as KBr pellets (left axis, red line) and Raman spectra (right axis, blue line) of complex **(2)**$PF_6.H_2O$.

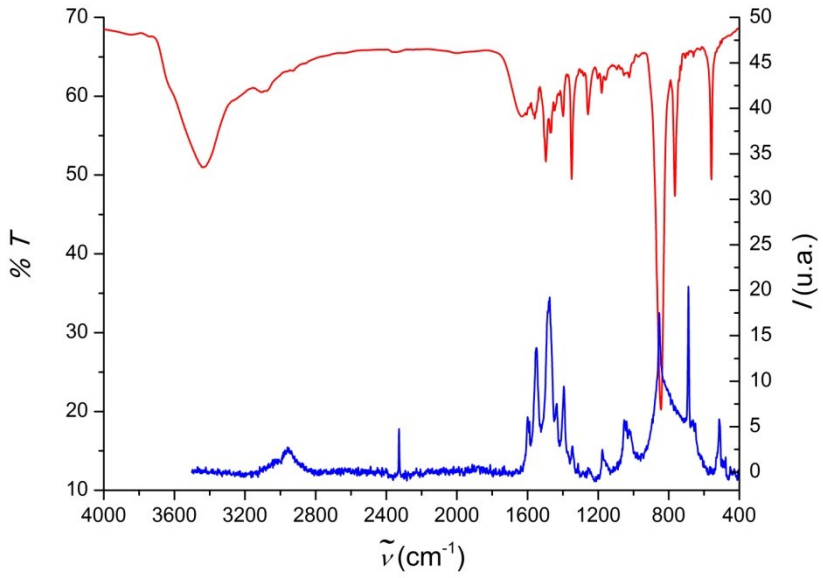

Figure S3. Infrared spectra as KBr pellets (left axis, red line) and Raman spectra (right axis, blue line) of complex **(4)**$(PF_6)_2$.

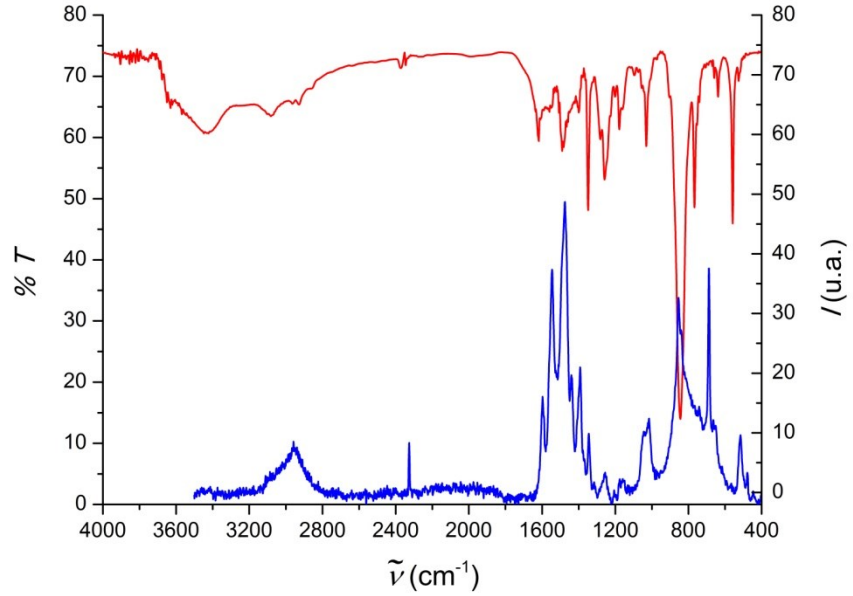

Figure S4. Infrared spectra as KBr pellets (left axis, red line) and Raman spectra (right axis, blue line) of complex **(5)**$(PF_6)_2.2H_2O$.

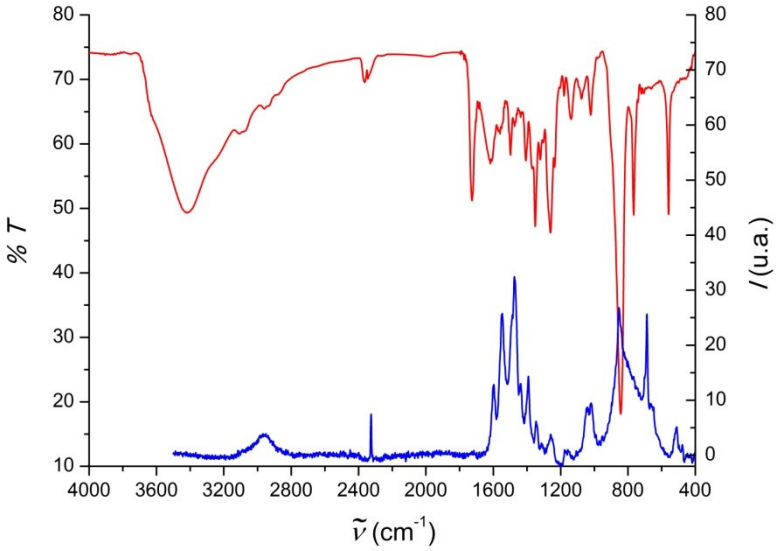

Figure S5. Infrared spectra as KBr pellets (left axis, red line) and Raman spectra (right axis, blue line) of complex **(6)**$(PF_6)_2.0.5H_2O$.

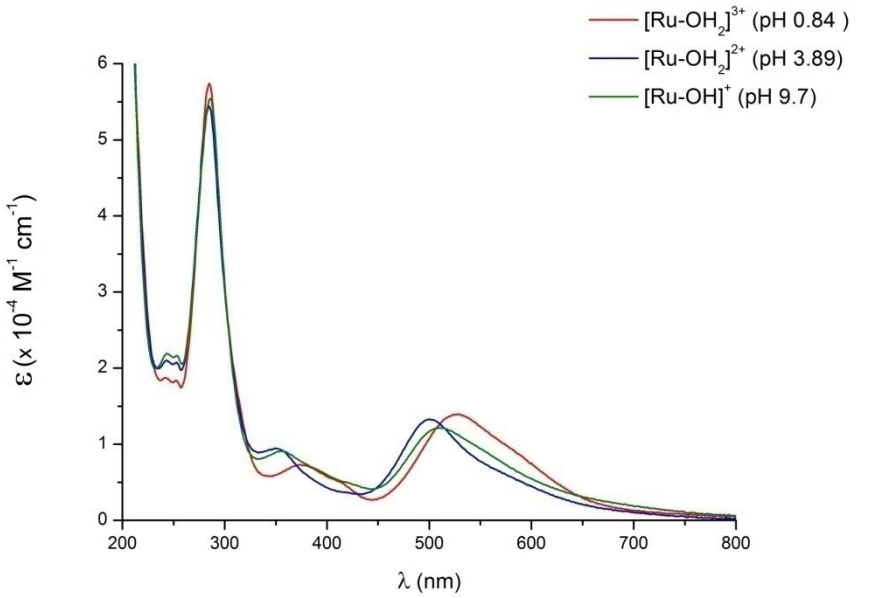

Figure S6. UV-visible spectra, in Britton and Robinson's buffer, of complexes **(4):** pH = 3.89 (blue line**)** and pH = 0.84 (red line); pH = 9.7 $[Ru(tptz)(bpy)(OH)]^{+}$.

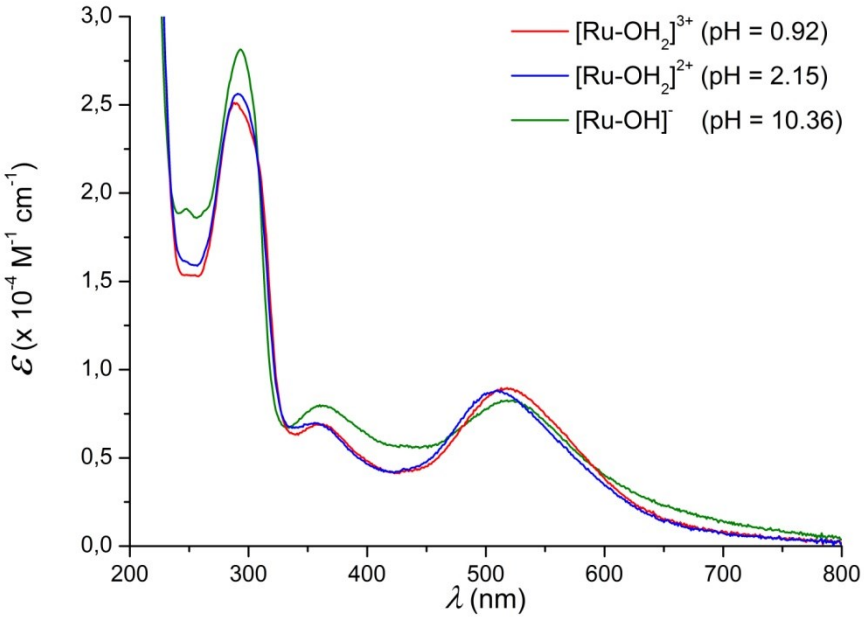

Figure S7. UV-visible spectra, in Britton and Robinson's buffer, of complexes **(6):** pH = 2.15 (blue line**)** and pH = 0.92 (red line); pH = 10.36 $[Ru(tptz)(dcb)(OH)]^{-}$.

a)

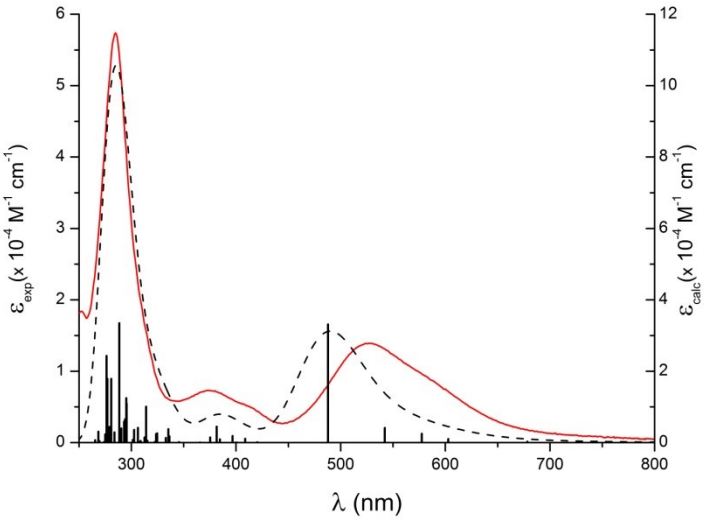

b)

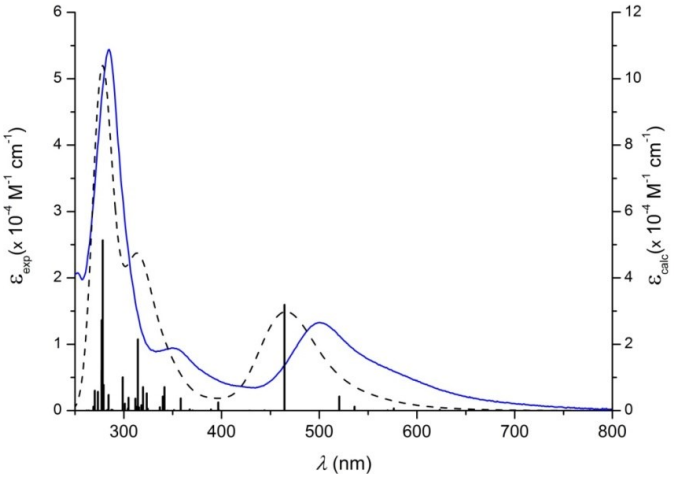

c)

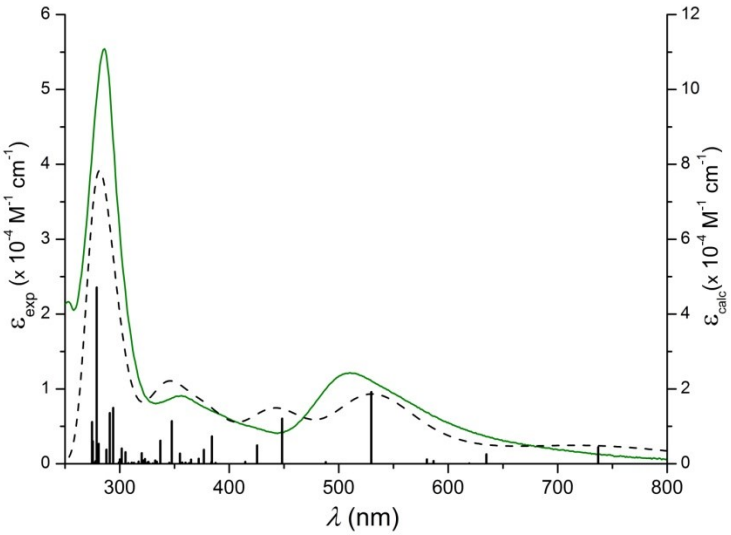

Figure S8. UV-Vis spectra, experimental (solid colored lines) and calculated by TD-DFT (black dash lines) together with the electronic transitions calculated (vertical lines). (a) $[Ru(tptzH)(bpy)(OH_2)]^{3+}$ (experimental spectrum at pH = 0.84) (b) $[Ru(tptz)(bpy)(OH_2)]^{2+}$ (pH = 3.89) (c)$[Ru(tptz)(bpy)(OH)]^{+}$ (pH = 9.7).

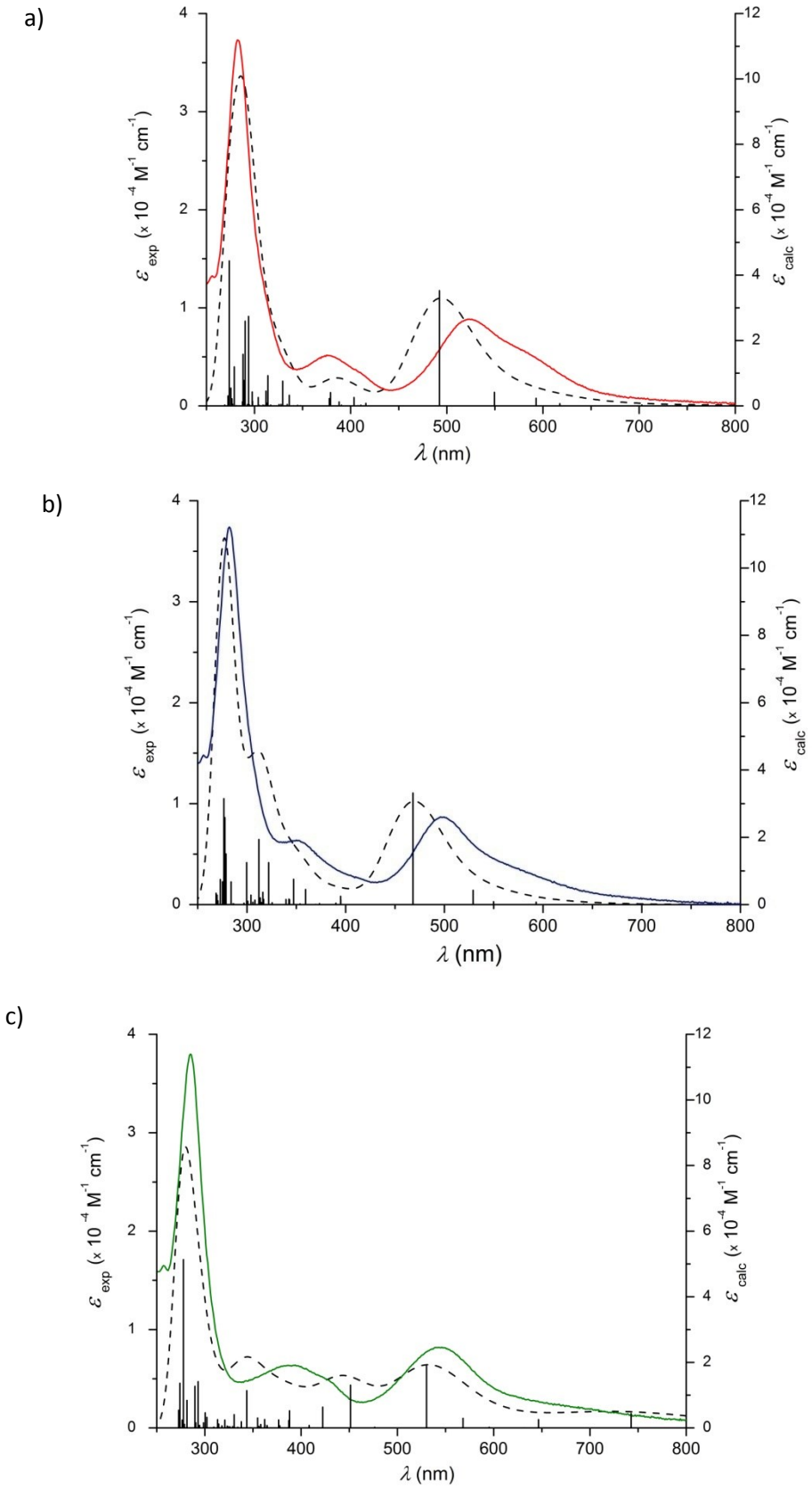

Figure S9. UV-Vis spectra, experimental (solid colored lines) and calculated by TD-DFT (black dash lines) together with the electronic transitions calculated (vertical lines). (a) $[Ru(tptzH)(dmb)(OH_2)]^{3+}$ (experimental spectrum at pH = 0.92); (b) $[Ru(tptz)(dmb)(OH_2)]^{2+}$ (pH = 3.89); (c) $[Ru(tptz)(dmb)(OH)]^{+}$ (pH = 12.16).

a)

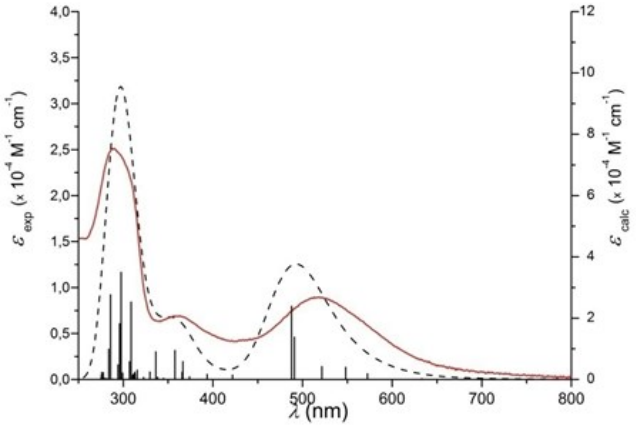

b)

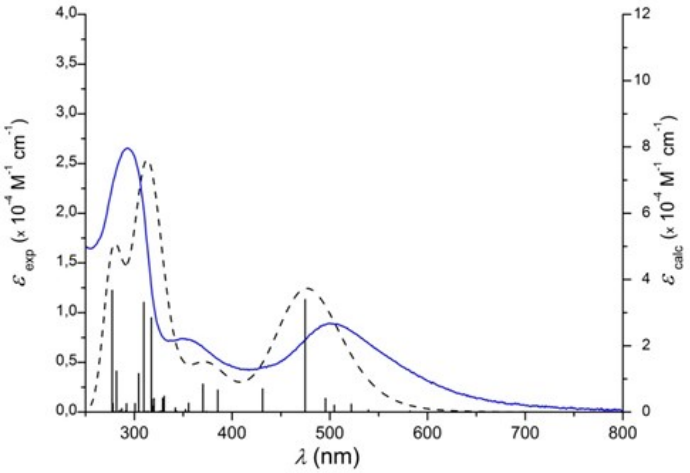

c)

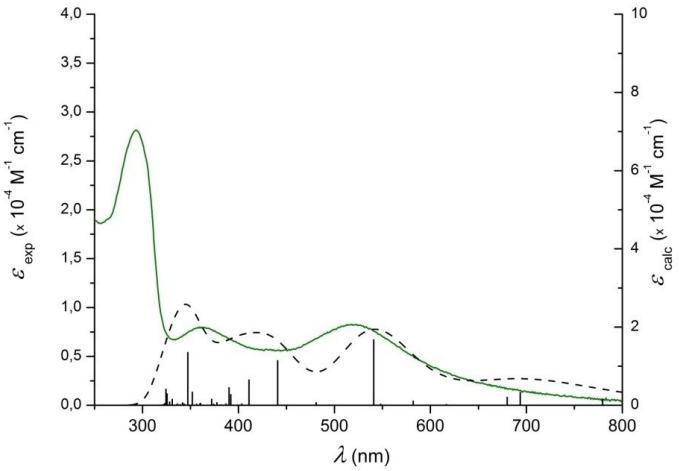

Figure S10. UV-Vis spectra, experimental (solid colored lines) and calculated by TD-DFT (black dash lines) together with the electronic transitions calculated (vertical lines). (a) $[Ru(tptzH)(dcb)(OH_2)]^{3+}$ (experimental spectrum at pH = 0.92); (b) $[Ru(tptz)(dcb)(OH_2)]^{2+}$ (pH = 2.15); (c) $[Ru(tptz)(dcb^{2-})(OH)]^{-}$ (pH = 10.36).

(a)

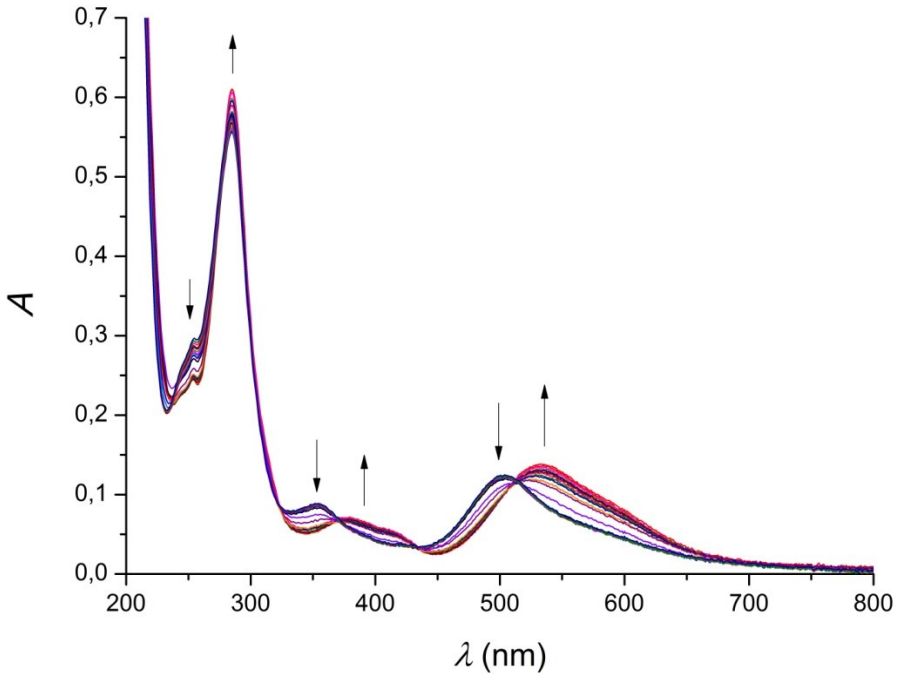

(b)

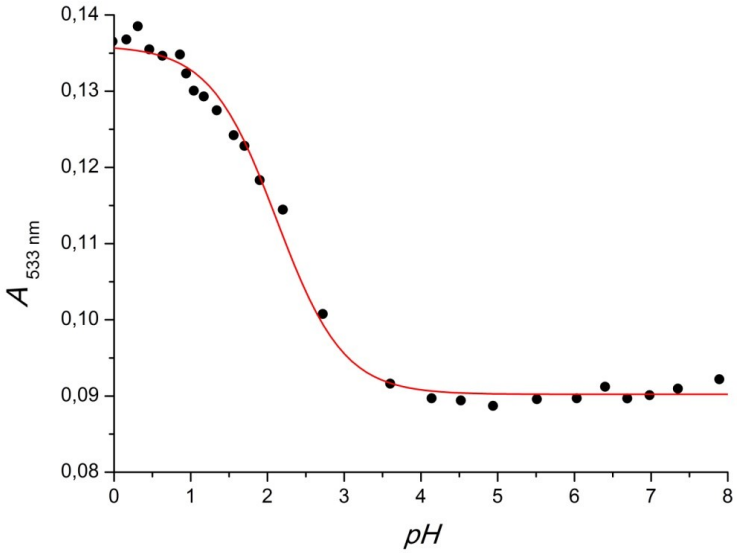

Figure S11. (a): UV-visible spectra of acid-base titration of complex **(1)** in Britton and Robinson's buffer, C = $2.2.10^{-5}$ M, 7.89 > pH > 0.31. **(b)** Absorbance at λ = 533 nm versus pH, red line is the fitting curve using a two-species model.

(a)

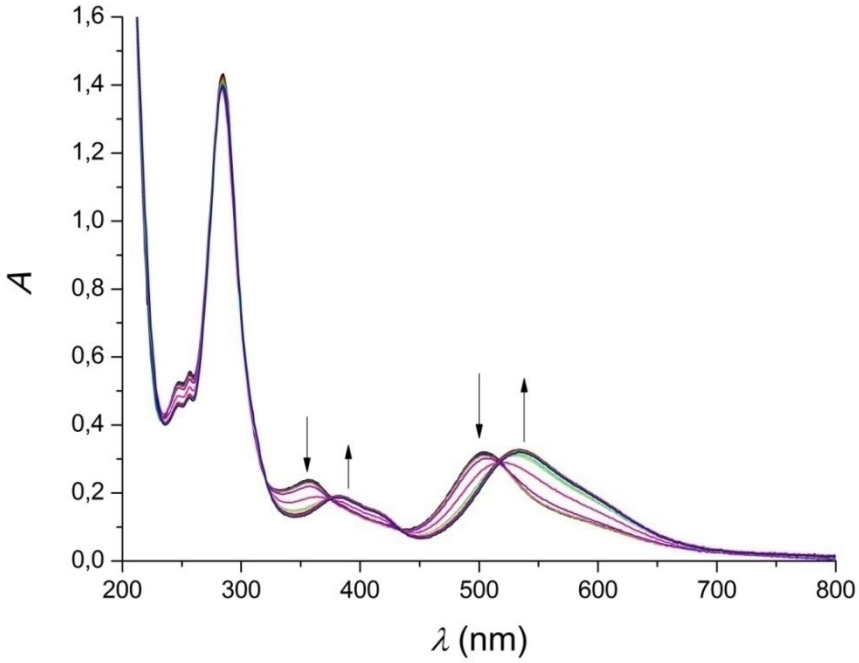

(b)

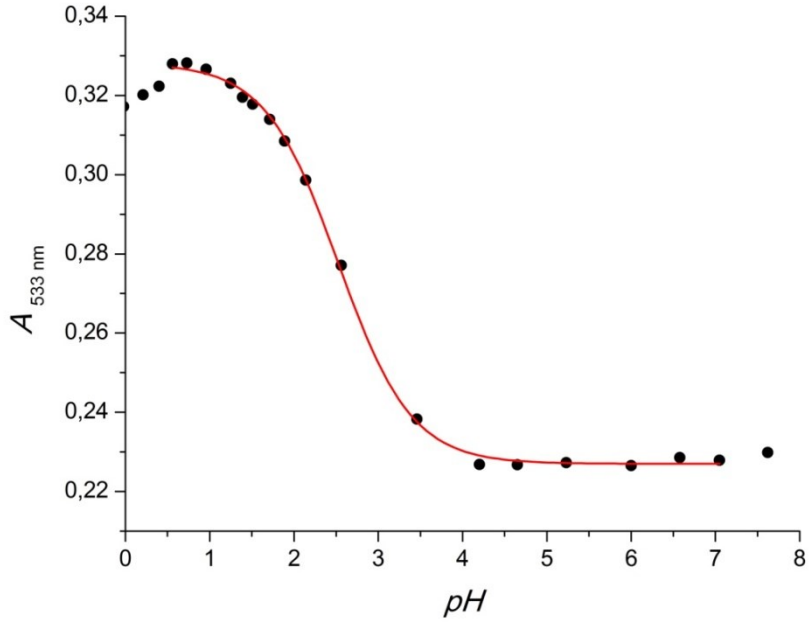

Figure S12. (a): UV-visible spectra of acid-base titration of complex **(2)** in Britton and Robinson's buffer, C = $4.3.10^{-5}$ M, 7.62 > pH > 0.21. **(b)** Absorbance at λ = 533 nm versus pH, red line is the fitting curve using a two-species model.

(a)

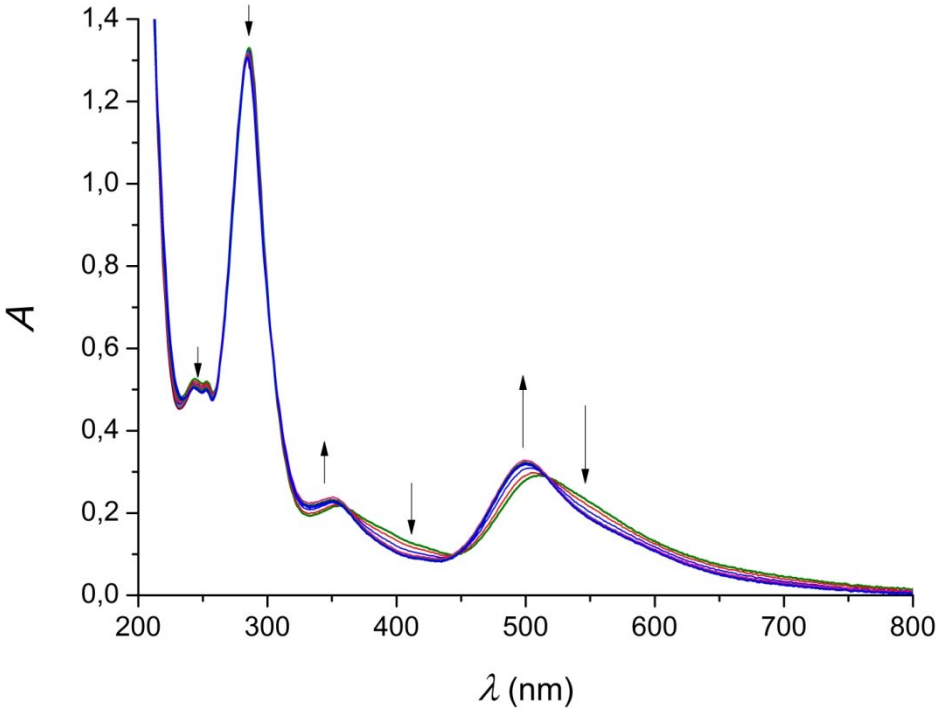
1,4
1,2
1,0
0,8
0,6
0,4
0,2
0,0
A
200
300
400
500
600
700
800
λ (nm)

(b)

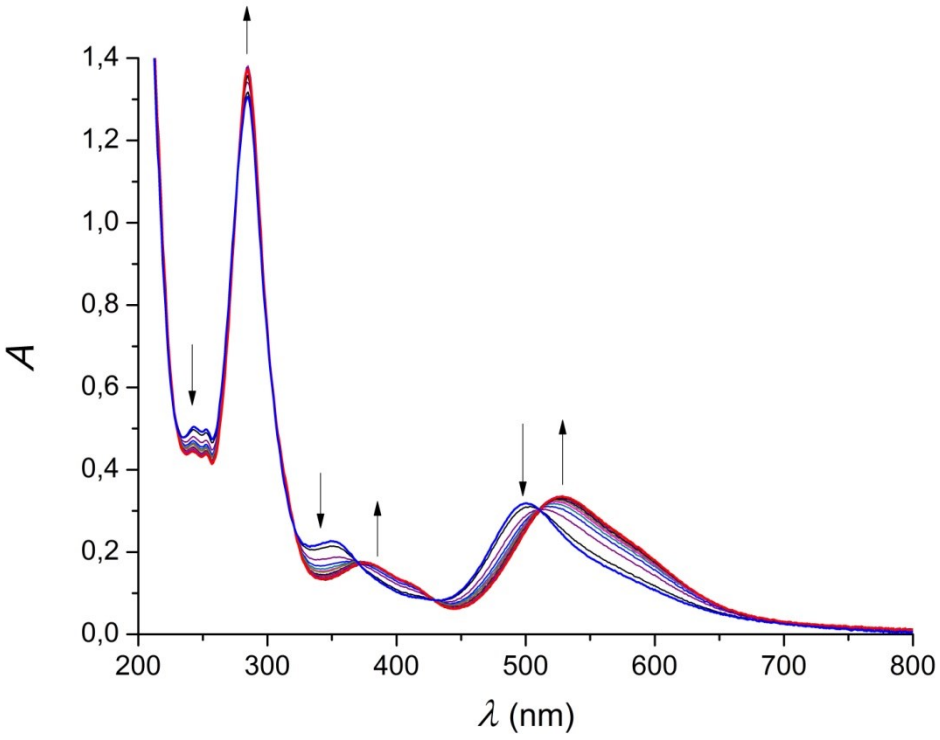
1,4
1,2
1,0
0,8
0,6
0,4
0,2
0,0
A
200
300
400
500
600
700
800
λ (nm)

(c)

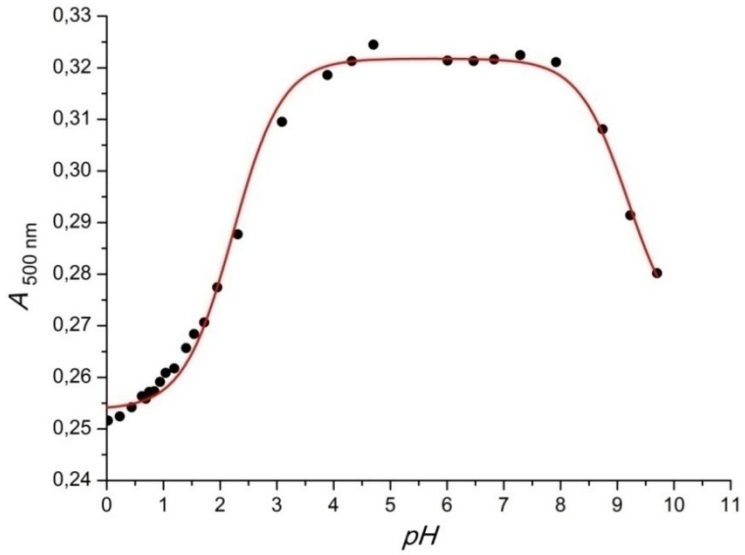

(d)

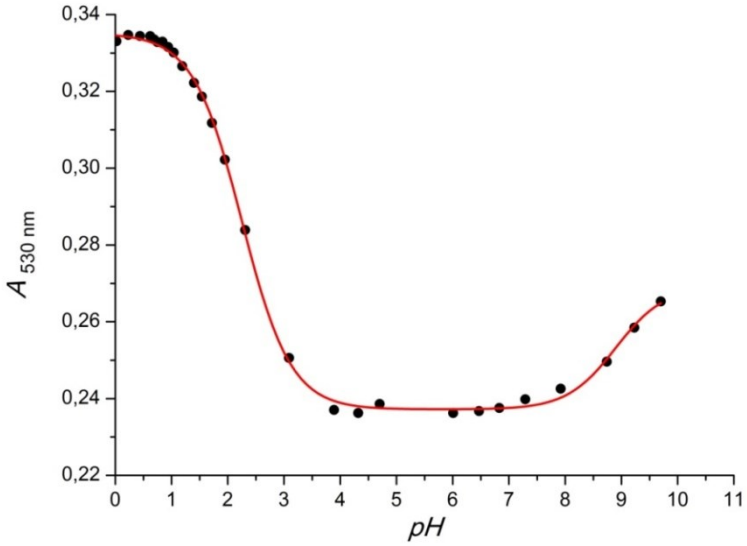

Figure S13. UV-visible spectra of acid-base titration of complex **(4)** in Britton and Robinson's buffer, C = $2.4.10^{-5}$ M. **(a)** 9.70 > pH > 3.89 (isosbestic points at λ = 515, 444, 360 and 304 nm) and **(b)** 3.89 > pH > 0 (isosbestic points at λ = 510, 430, 370, 320 and 278 nm). **(c)** Absorbance at λ = 500 nm versus pH, red line is the fitting curve using a two-species model (pKa_{tptz} = 2.22 ±0.05; pKa_{OH_2} = 9.19 ±0.05). **(d)** Absorbance at λ = 530 nm versus pH, red line is the fitting using a two-species model (pKa_{tptz} = 2.25 ± 0.05; pKa_{OH_2} = 8.90 ± 0.05).

(a)

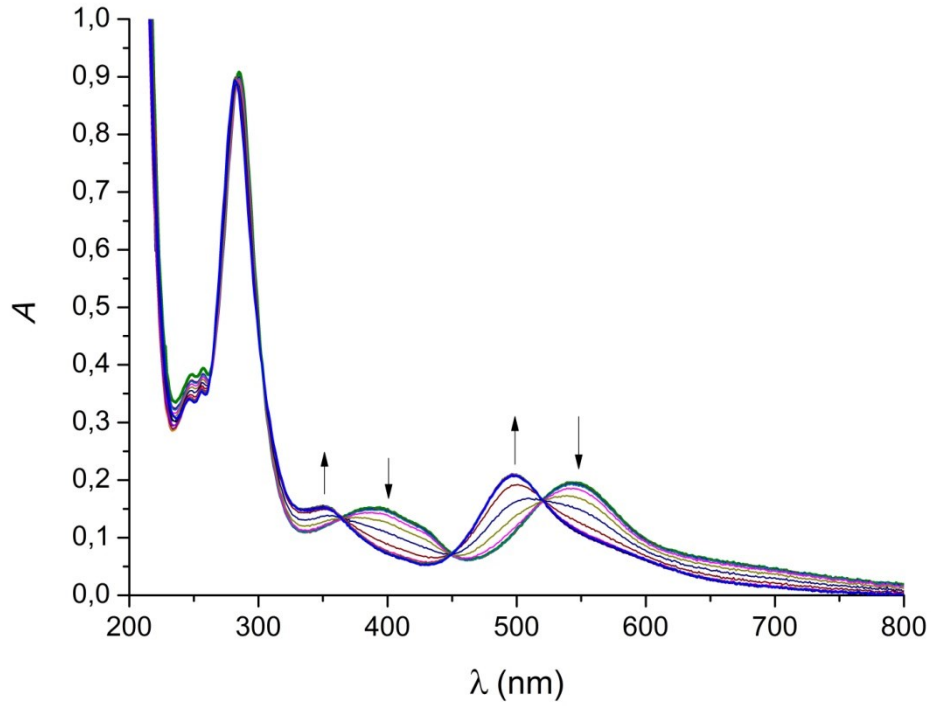
1,0
0,9
0,8
0,7
0,6
0,5
0,4
0,3
0,2
0,1
0,0
A
200
300
400
500
600
700
800
λ (nm)

(b)

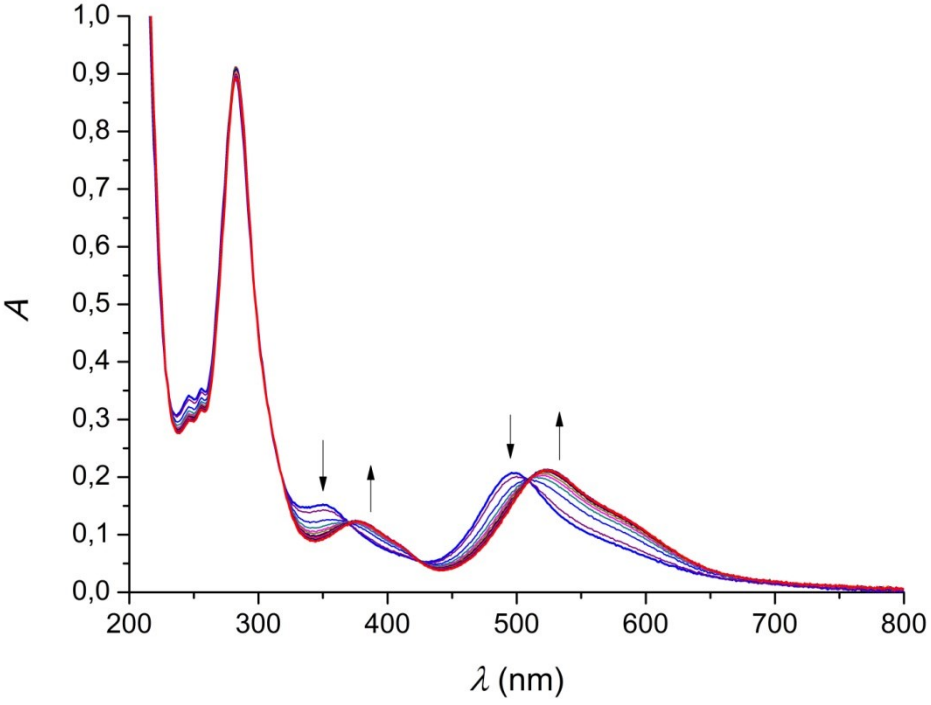
1,0
0,9
0,8
0,7
0,6
0,5
0,4
0,3
0,2
0,1
0,0
A
200
300
400
500
600
700
800
λ (nm)

(c)

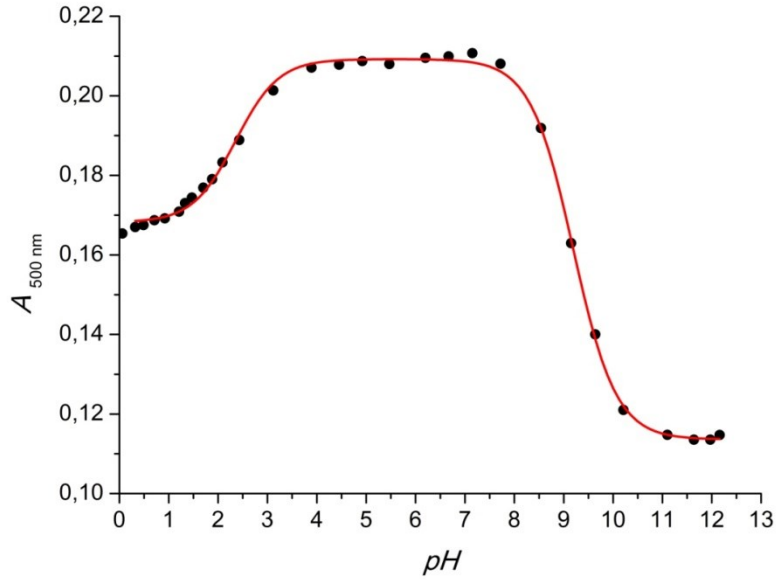

d)

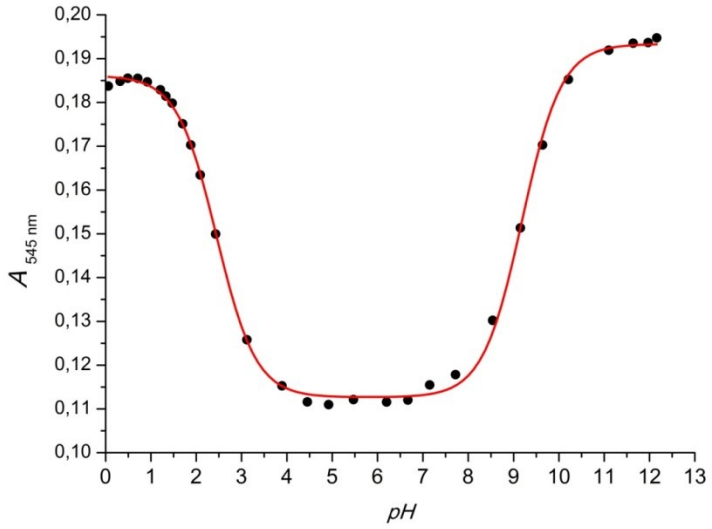

Figure S14. UV-visible spectra of acid-base titration of complex **(4)** in Britton and Robinson's buffer, C = $2.4.10^{-5}$ M **(a)** 12.16 > pH > 3.89 (isosbestic points at λ = 520, 448, 365, 303, 283 and 264 nm) and **(b)** 3.89 > pH > 0.06 (isosbestic points at λ = 508, 428 and 369 nm) **(c)** Absorbance at λ = 500 nm versus pH, red line is the fitting using a two-species model (pKa_{tptz} = 2.36 ±0.05; pKa_{OH_2} = 9.19±0.05). **(d)** Absorbance at λ = 545 nm versus pH, red line is the fitting using a two-species model (pKa_{tptz} = 2.45±0.05; pKa_{OH_2} = 9.19±0.05).

a)

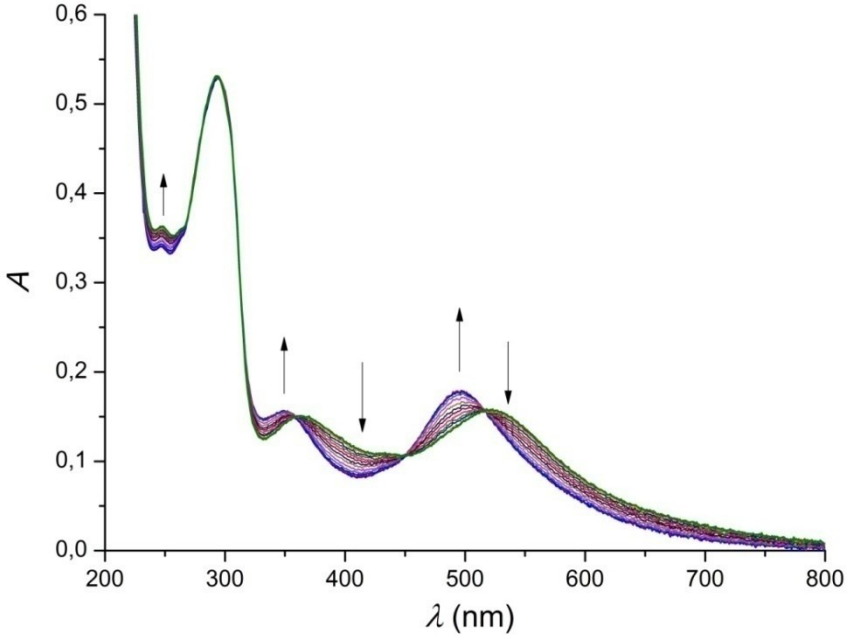
0,6
0,5
0,4
0,3
0,2
0,1
0,0
A
200
300
400
500
600
700
800
λ (nm)

b)

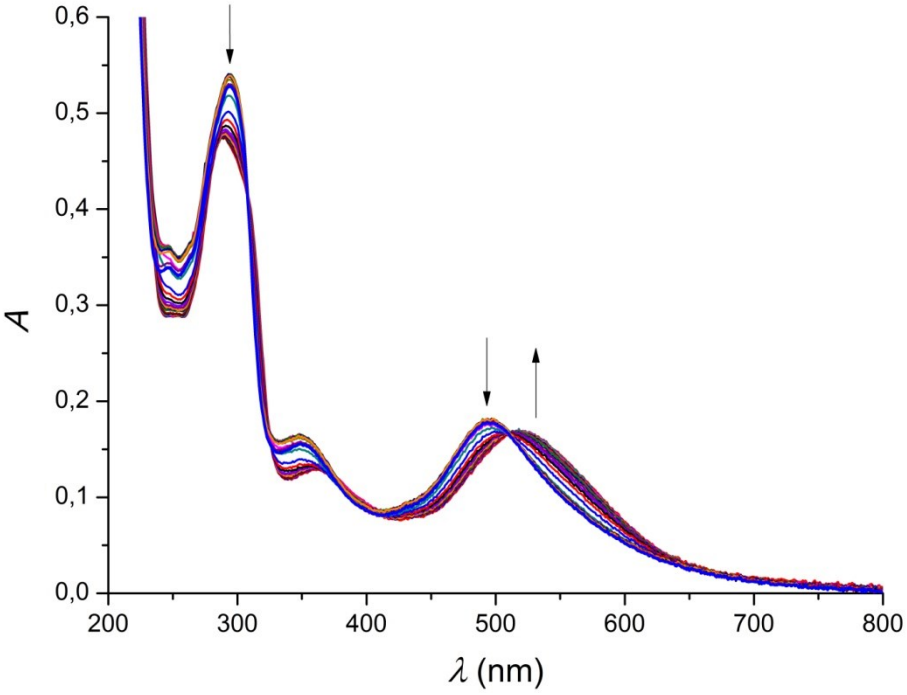
0,6
0,5
0,4
0,3
0,2
0,1
0,0
A
200
300
400
500
600
700
800
λ (nm)

c)

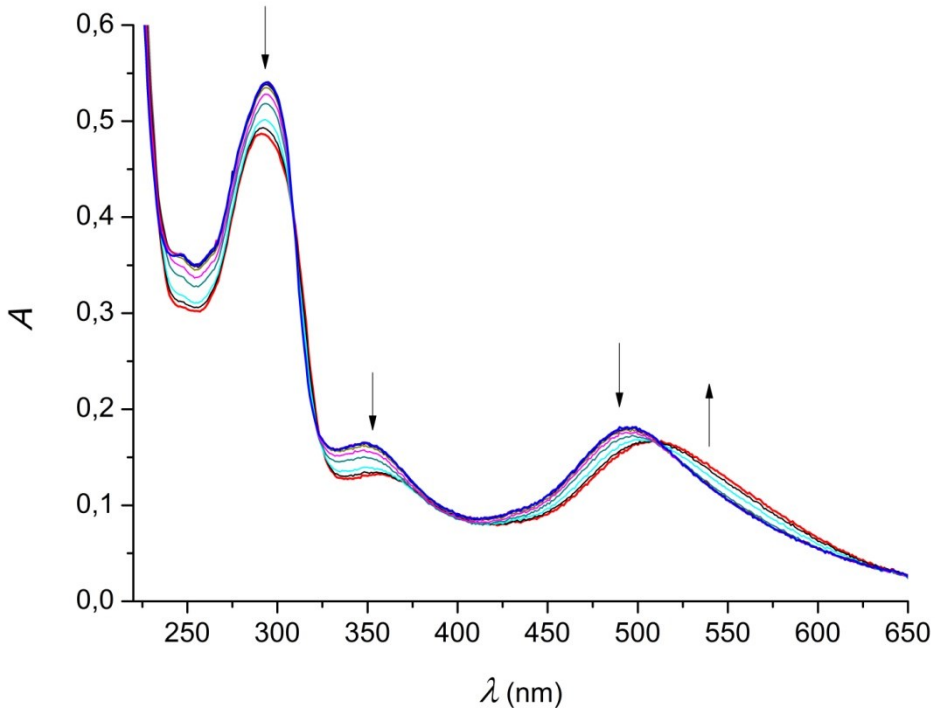
0,6
0,5
0,4
0,3
0,2
0,1
0,0
A
250
300
350
400
450
500
550
600
650
λ (nm)

d)

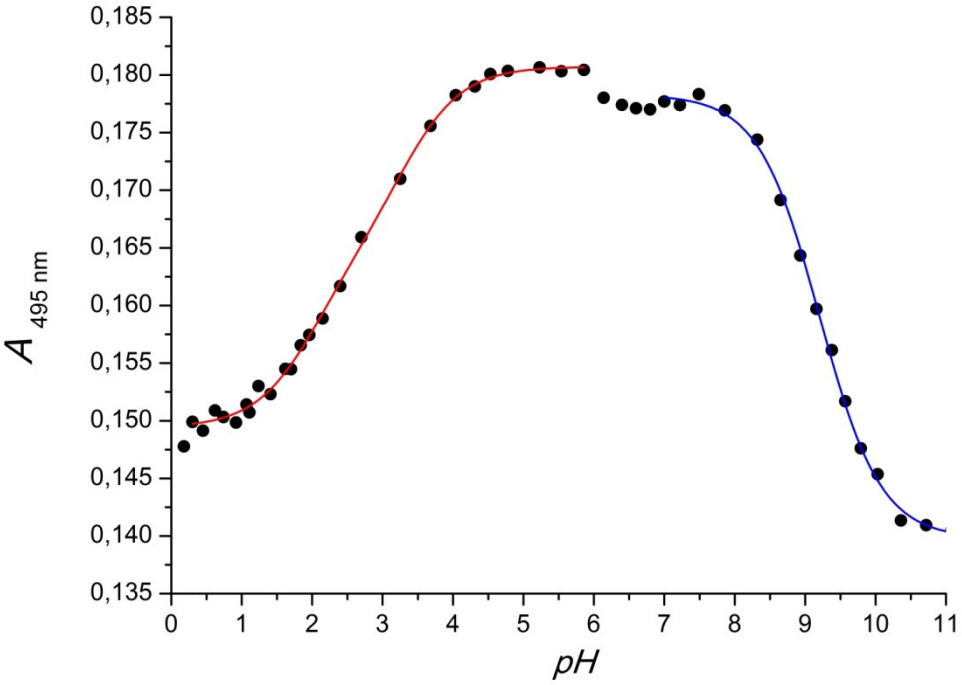
0,185
0,180
0,175
0,170
0,165
0,160
0,155
0,150
0,145
0,140
0,135
A 495 nm
0
1
2
3
4
5
6
7
8
9
10
11
pH

e)

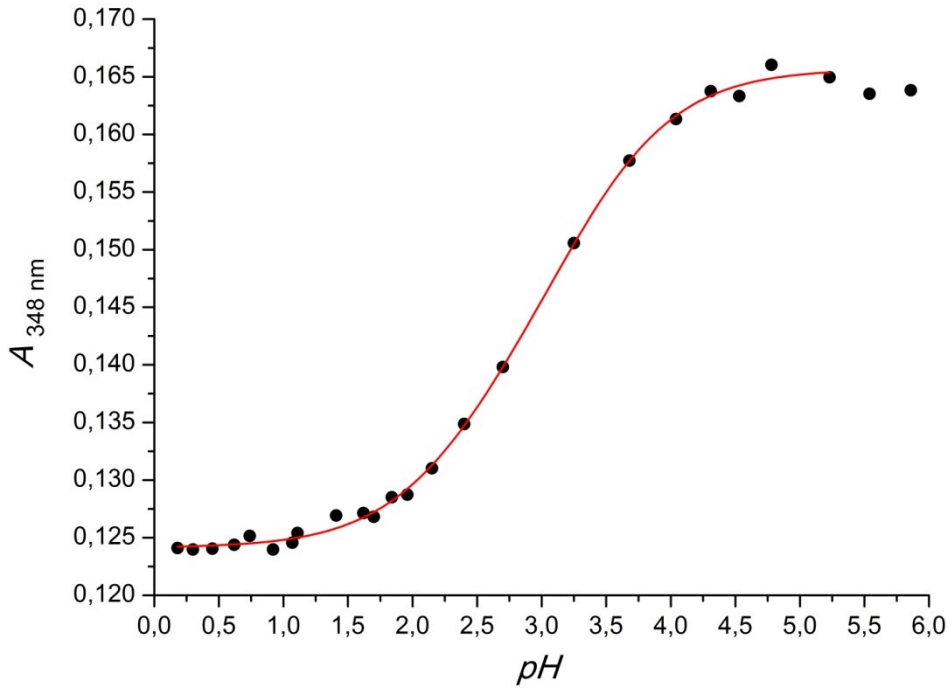
0,170
0,165
0,160
0,155
0,150
0,145
0,140
0,135
0,130
0,125
0,120
A 348 nm
0,0 0,5 1,0 1,5 2,0 2,5 3,0 3,5 4,0 4,5 5,0 5,5 6,0
pH

f)

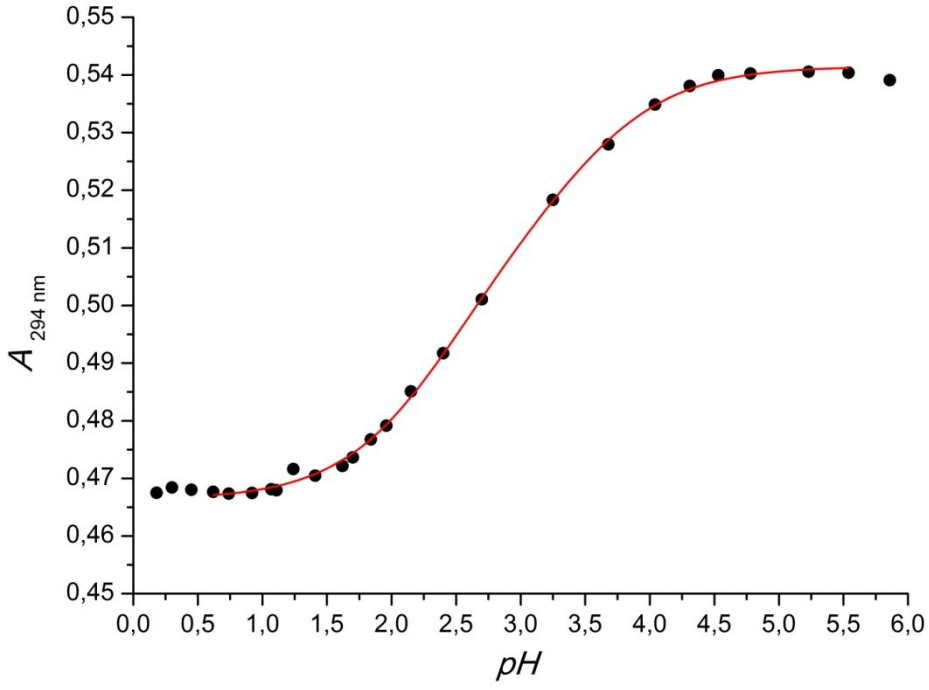
0,55
0,54
0,53
0,52
0,51
0,50
0,49
0,48
0,47
0,46
0,45
A 294 nm
0,0 0,5 1,0 1,5 2,0 2,5 3,0 3,5 4,0 4,5 5,0 5,5 6,0
pH

Figure S15. UV-visible spectra of acid-base titration of complex **(6)** in Britton and Robinson's buffer, C = $2.4.10^{-5}$ M **(a)** 11.02 > pH > 7.22 (isosbestic points at λ = 515, 450, 359 and 268 nm); **(b)** 7.01 > pH > 0.18 (isosbestic point at λ = 510 nm) and **(c)** 5.23 > pH > 2.15. **(d)** Absorbance at λ = 495 nm versus pH, red line is the fitting using a three-species model ($pKa1_{COOH}$ = 3.33±0.05; pKa_{tptz} = 1.98±0.05), blue line is the fitting using a two-species model (pKa_{OH2} = 9.20±0.05). (e) Absorbance at λ = 348 nm versus pH, red line is the fitting using a three-species model ($pKa1_{COOH}$ = 3.32±0.05; $pKa2_{COOH}$ = 2.38±0.05). (f) Absorbance at λ = 294 nm versus pH, red line is the fitting using a three-species model ($pKa1_{COOH}$ = 3.46±0.05; $pKa2_{COOH}$ = 2.37±0.05).

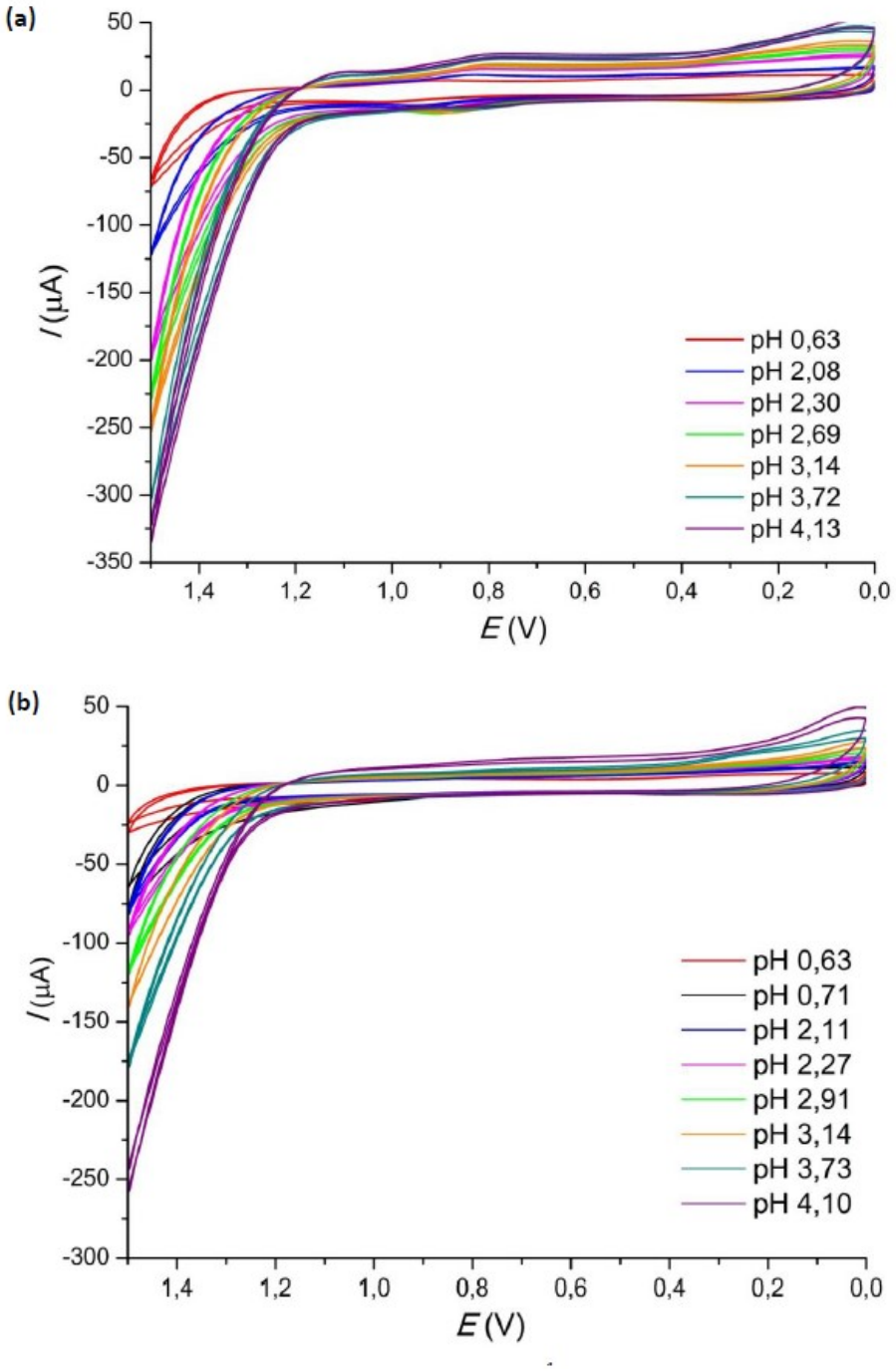

Figure S16. Cyclic voltammogram at v = 100 mV.s^{-1} for at acidic pH's in $HClO_4$ 0.1M and NaOH 0.1M with $NaClO_4$ (*I*=0.1M) : a) complex (**4)** b) supporting electrolyte. The potential values are referred to Ag/AgCl (3M NaCl).

a)

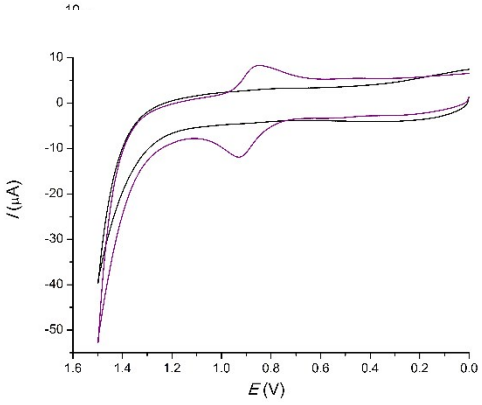

c)

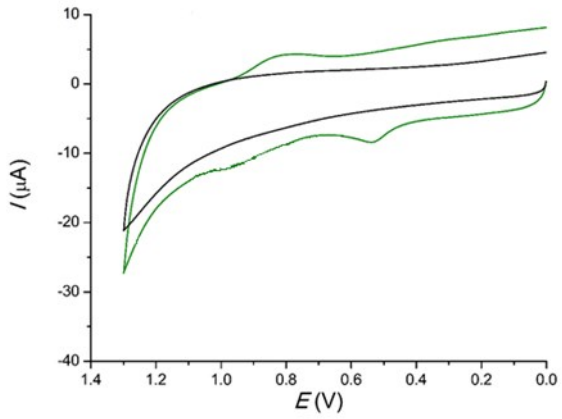

Figure S17 Cyclic voltammogram at v = 100 mV.s^{-1} for complex (4) at different pH's in $HClO_4$ 0.1M and NaOH 0.1M with $NaClO_4$ (*I*=0.1M) : a) pH = 1.5. b) pH = 5.2 c) 10.12 The supporting electrolyte is represented in black. The potential values are referred to Ag/AgCl (3M NaCl).

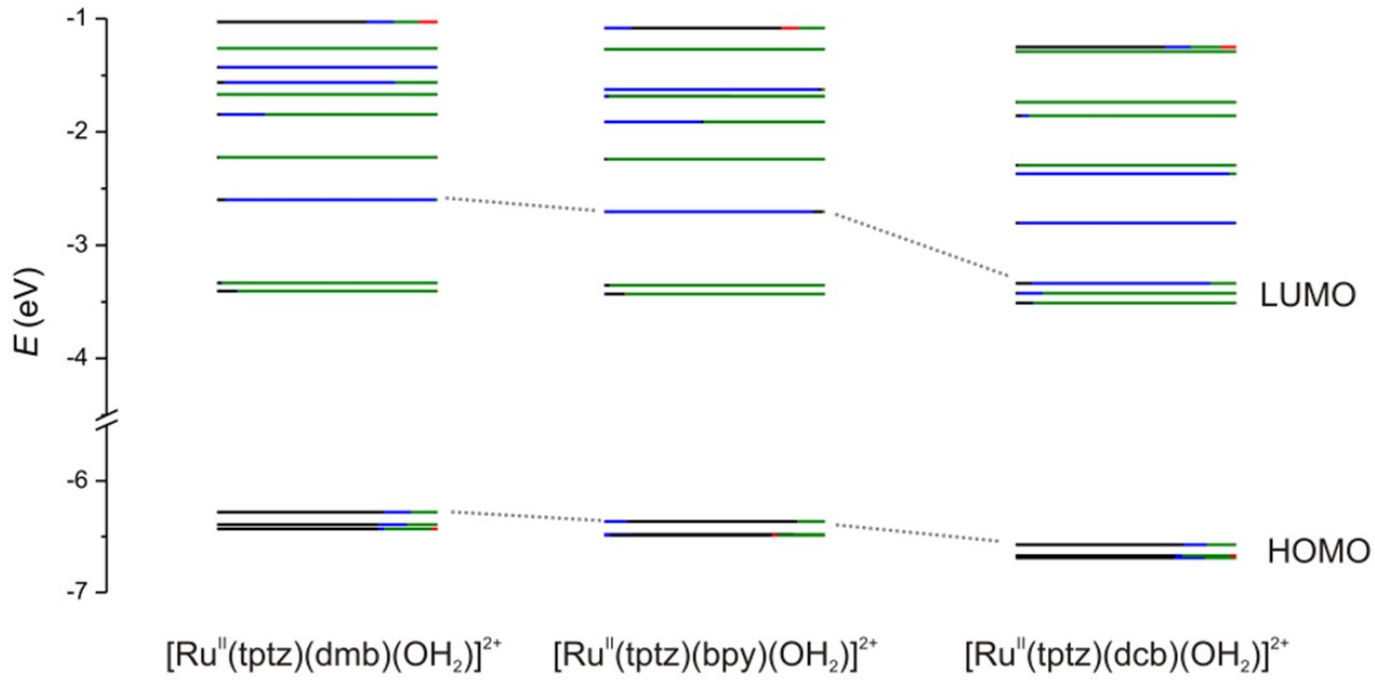

Figure S18. Orbital diagrams calculated by DFT. Different contributions of the groups are marked by different colors: RuII in black, bpy/dmb/dcb in blue, tptz in green and OH_2 in red. For the values of each contribution see Tables S1, S2 and S3.

a)

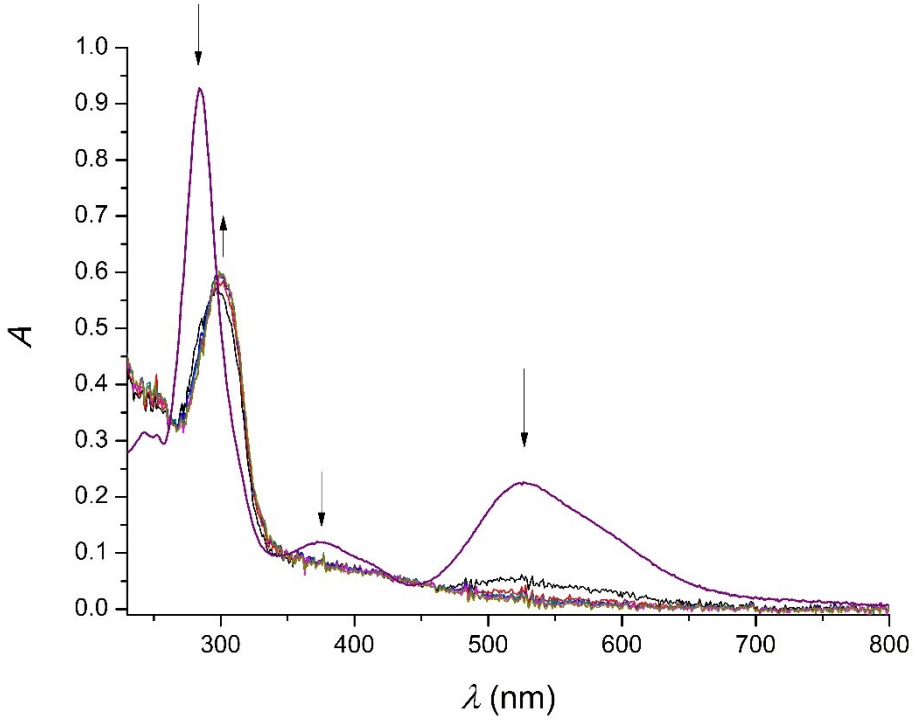
1.0
0.9
0.8
0.7
0.6
0.5
0.4
0.3
0.2
0.1
0.0
A
300
400
500
600
700
800
λ (nm)

b)

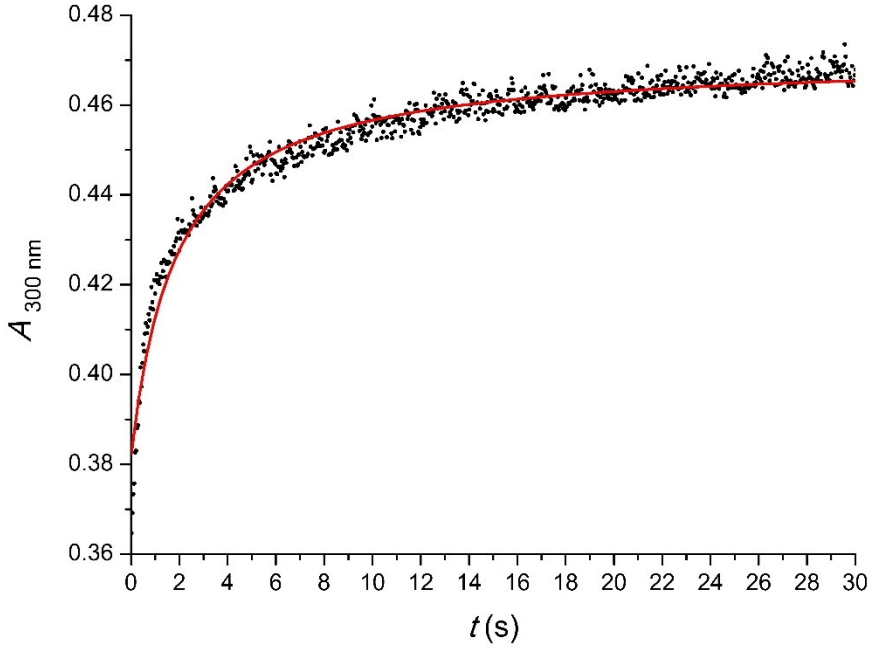
0.48
0.46
0.44
0.42
0.40
0.38
0.36
A 300 nm
0
2
4
6
8
10
12
14
16
18
20
22
24
26
28
30
t (s)

c)

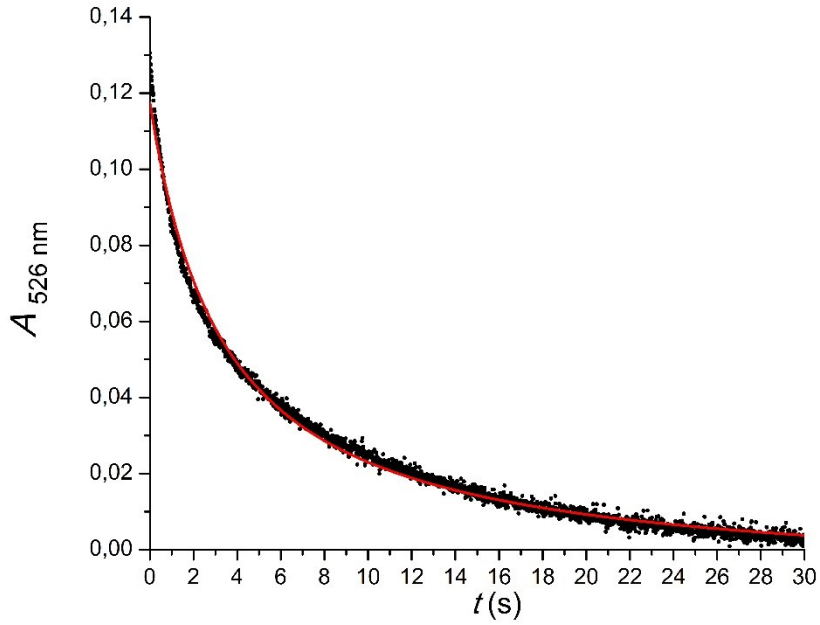

Figure S19. (a): UV-Visible spectra after the addition of 2 equiv of Ce^{IV} to [Ru(tptzH)(bpy)$(OH_2)]^{3+}$, C =1.06x10^{-5} M in $HClO_4$ 0.1 M; Δt = 9 s. **(b)** Absorbance at 300 nm vs. time. (c) Absorbance at 526 nm vs. time. Experimental values in black and curve fitted in red.

a)

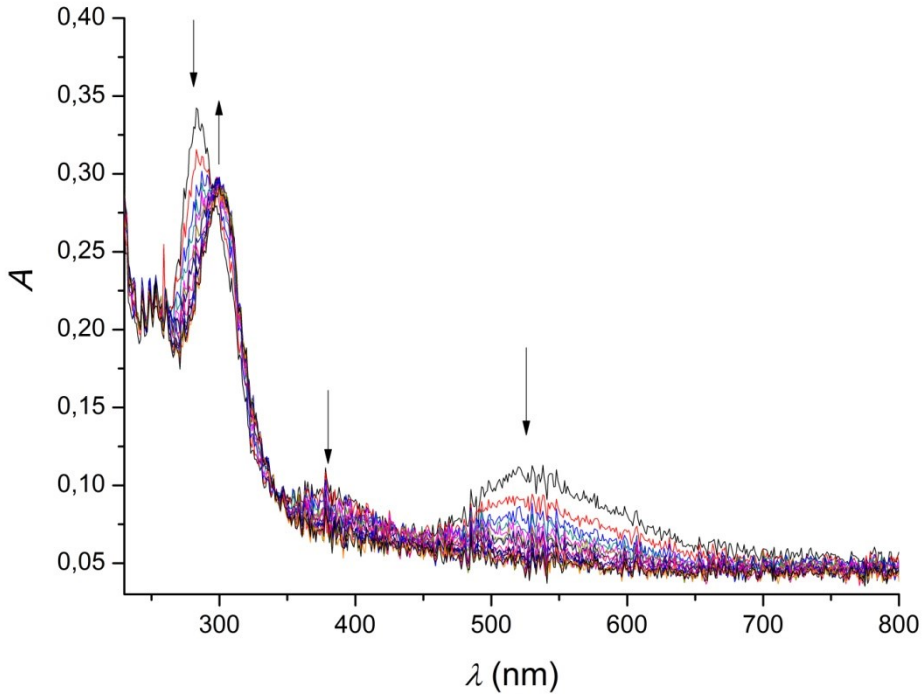
0,40
0,35
0,30
0,25
0,20
0,15
0,10
0,05
A
300
400
500
600
700
800
λ (nm)

b)

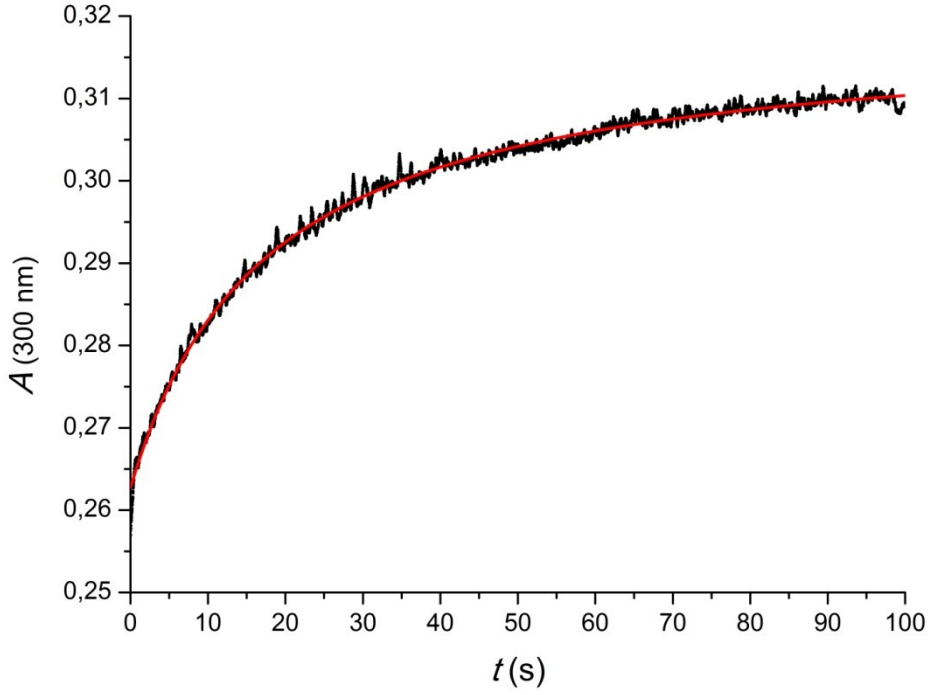
0,32
0,31
0,30
0,29
0,28
0,27
0,26
0,25
A (300 nm)
0
10
20
30
40
50
60
70
80
90
100
t (s)

c)

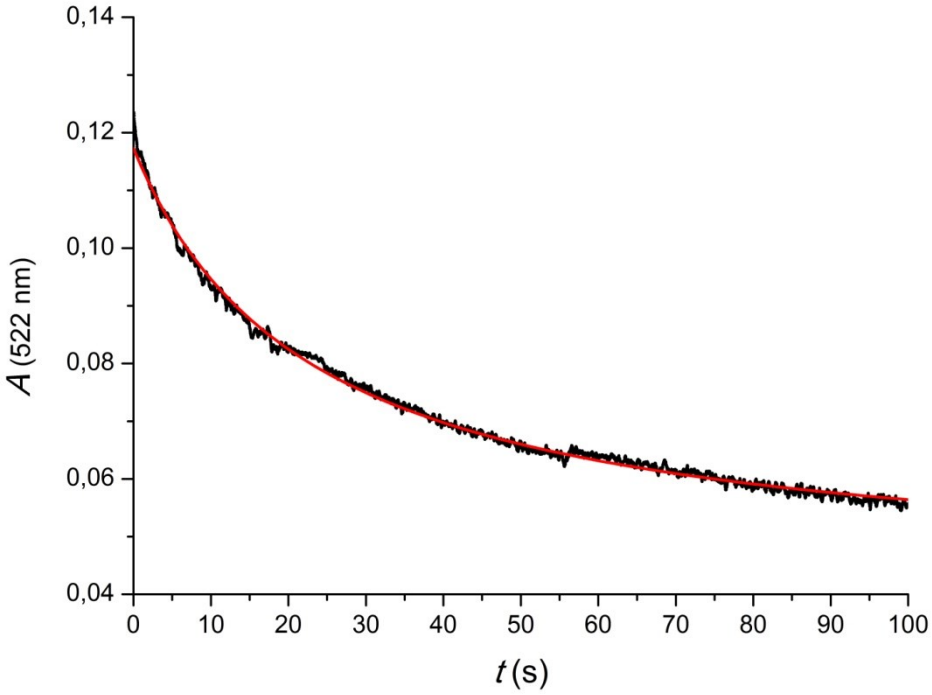

Figure S20. (a): UV-Visible spectra after the addition of 2 equiv of Ce^{IV} to $[Ru(tptzH)(dmb)(OH_2)]^{3+}$, C =1.06x10^{-5} M in $HClO_4$ 0.1 M; Δt = 9 s. **(b)** Absorbance at 300 nm vs. time. (c) Absorbance at 522 nm vs. time. Experimental values in black and curve fitted in red.

a)

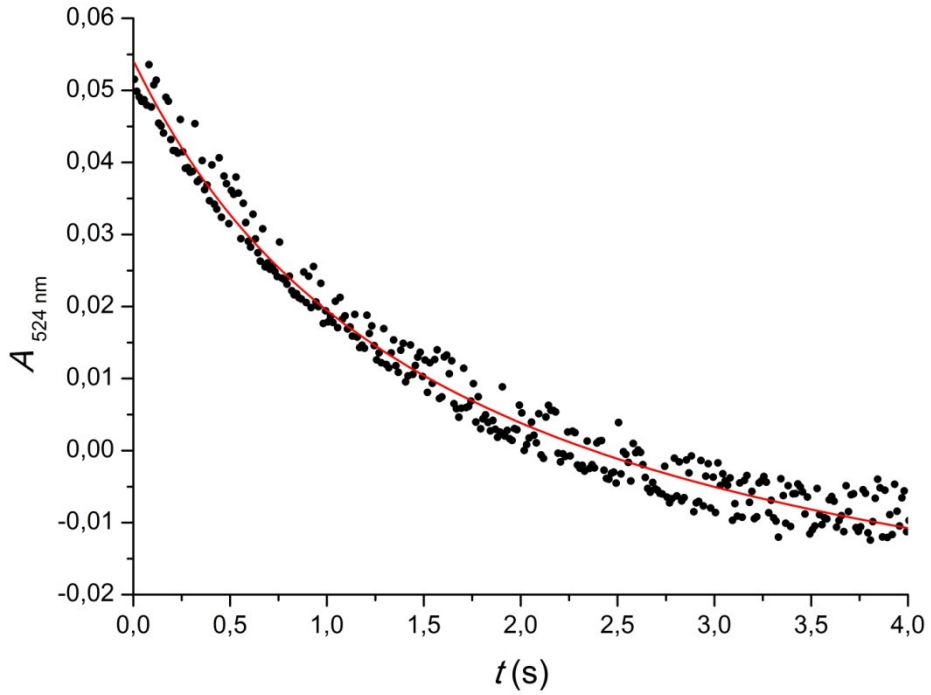
0,06
0,05
0,04
0,03
0,02
0,01
0,00
-0,01
-0,02
A 524 nm
0,0
0,5
1,0
1,5
2,0
2,5
3,0
3,5
4,0
t (s)

b)

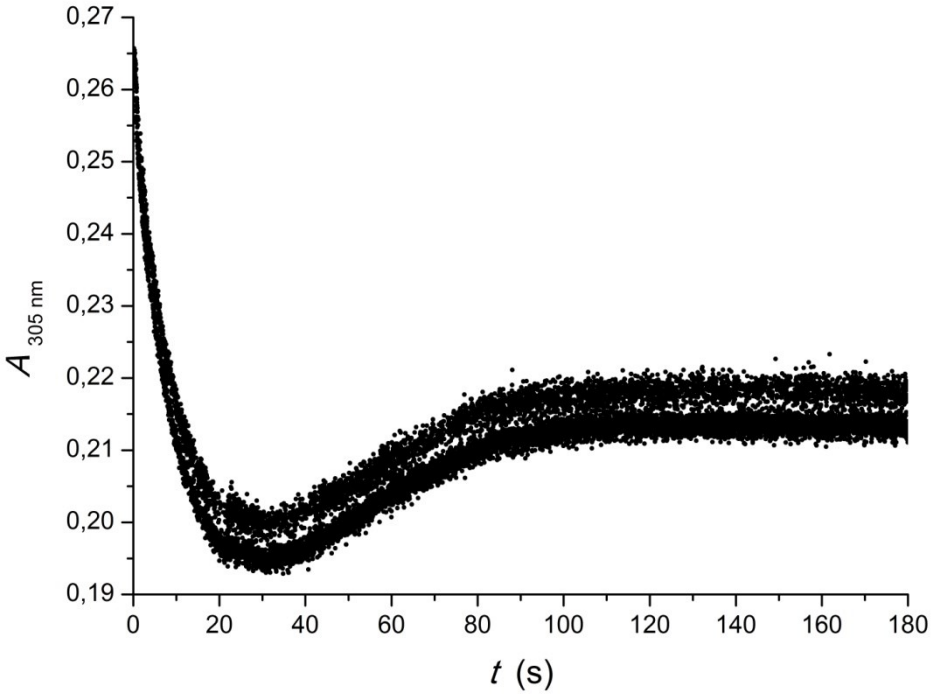
0,27
0,26
0,25
0,24
0,23
0,22
0,21
0,20
0,19
A 305 nm
0
20
40
60
80
100
120
140
160
180
t (s)

c)

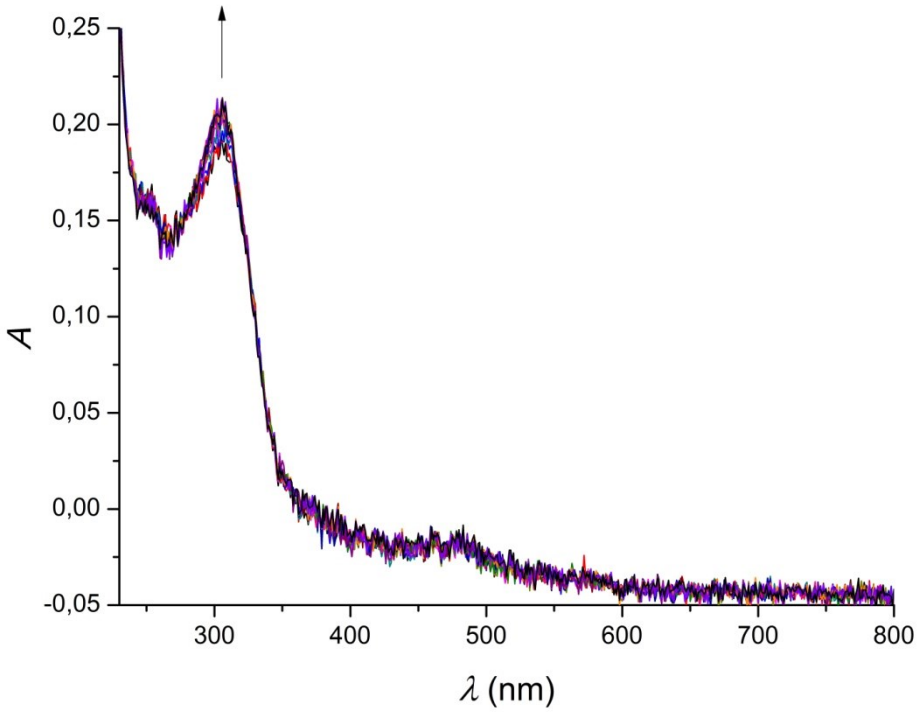

Figure S21. (a) Absorbance at 524 nm vs. time after the addition of 2 equiv of Ce^{IV} to $[Ru(tptzH)(dcb)(OH_2)]^{3+}$, C = 1.06x10^{-5} M in $HClO_4$ 0.1 M. Experimental values in black and curve fitted in red. **(b)** Absorbance at 305 nm vs. time. **(c)** UV-visible spectra between 30 and 180 second; Δt = 9 s.

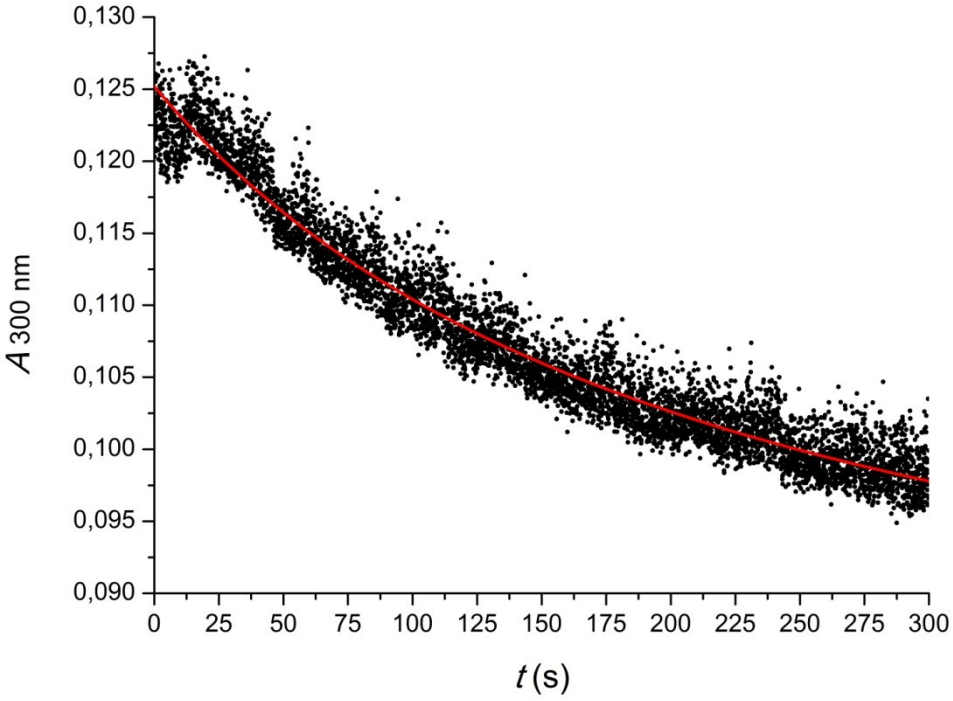

Figure S22. Absorbance at 300 nm vs. time after the addition of 1 equiv of Ce^{IV} to $[Ru^{IV}(tptzH)(bpy)(O)]^{3+}$, C =1.6x10^{-5} M, in $HClO_4$ 0.1 M.

a)

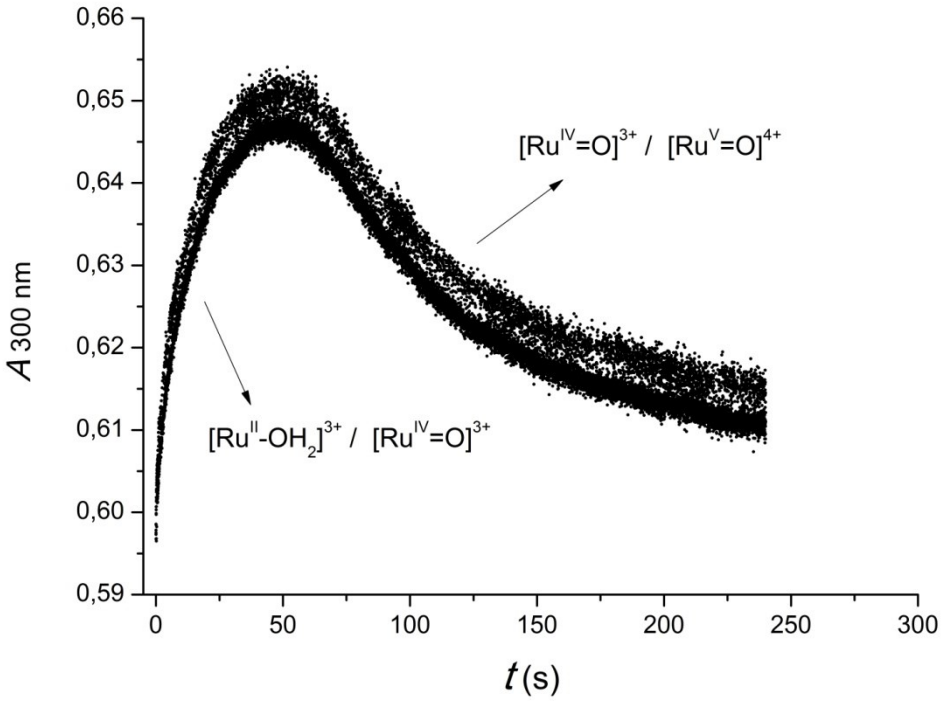
0,66
0,65
0,64
0,63
0,62
0,61
0,60
0,59
A 300 nm
0
50
100
150
200
250
300
t (s)
[Ru^IV=O]^3+ / [Ru^V=O]^4+
[Ru^II-OH2]^3+ / [Ru^IV=O]^3+

b)

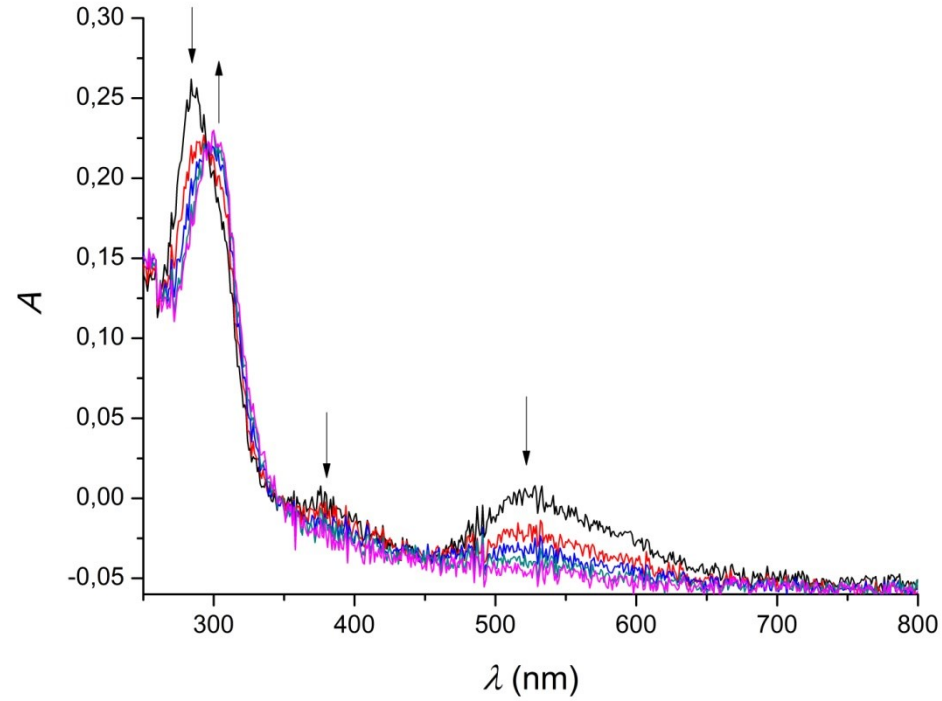
0,30
0,25
0,20
0,15
0,10
0,05
0,00
-0,05
A
300
400
500
600
700
800
λ (nm)

c)

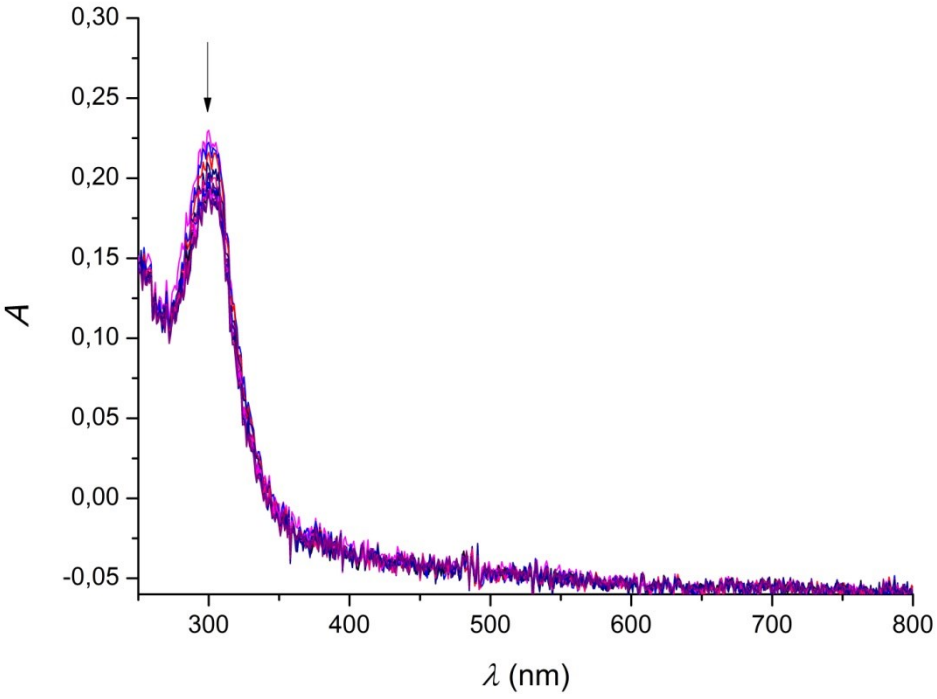

Figure S23. (a): Absorbance at 300 nm vs. time after the addition of 3 equiv of Ce^{IV} to $[Ru(tptzH)(dmb)(OH_2)]^{3+}$, C =1.06x10^{-5} M in $HClO_4$ 0.1 M**. (b)** UV-visible spectra of the reaction until 45 s. Δt = 9 s. **(c)** UV-visible spectra from 45 s to 5 min. Δt = 9 s.

a)

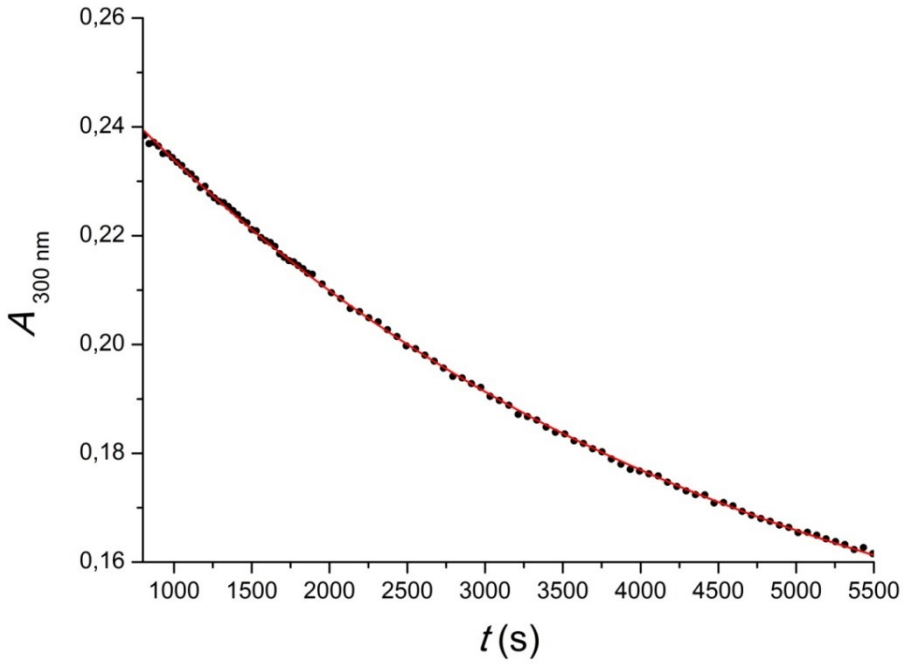

b)

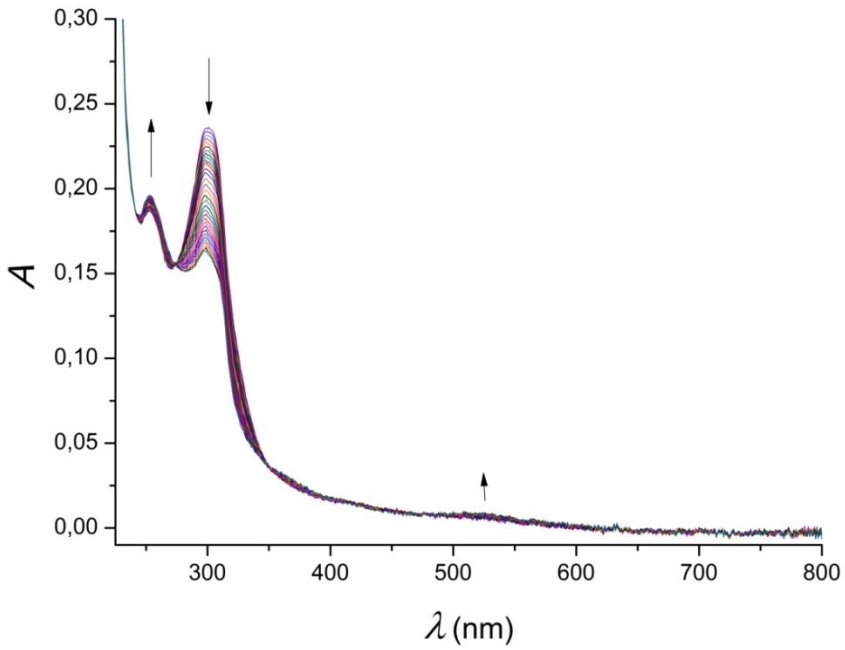

Figure S24. (a): Absorbance at 300 nm vs. time after the addition of 3 equiv of Ce^{IV} to $[Ru(tptzH)(dmb)(OH_2)]^{3+}$, C =1.06x10^{-5} M in $HClO_4$ 0.1 M in the time range from 950 to 5500 s; experimental values (black dots) and fitting with exponential function of first order (red line). **(b)** UV-visible spectra corresponding to that time interval.

a)

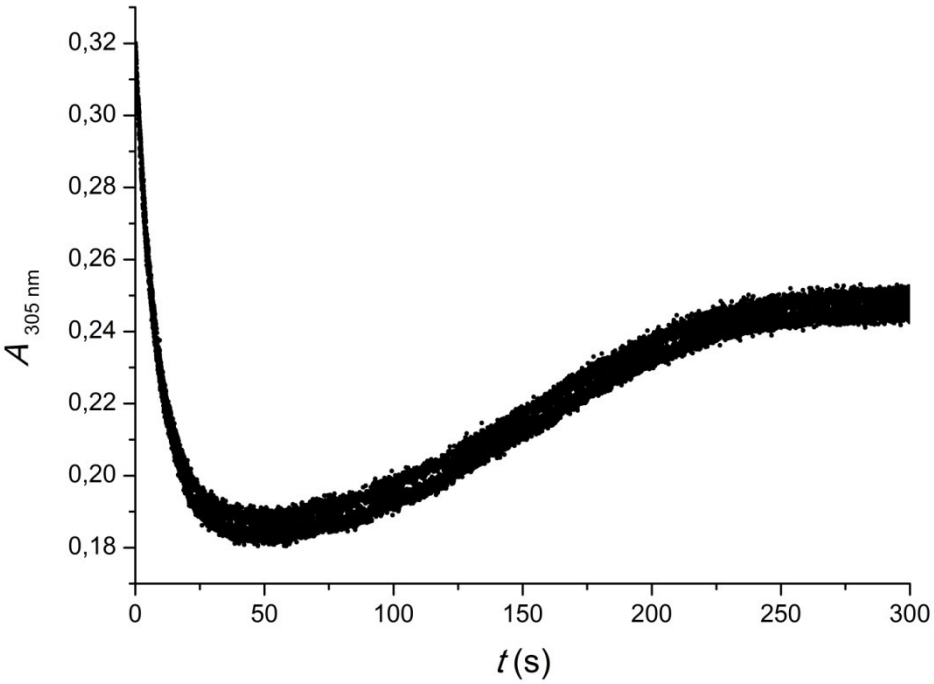
0,32
0,30
0,28
0,26
0,24
0,22
0,20
0,18
A 305 nm
0
50
100
150
200
250
300
t (s)

b)

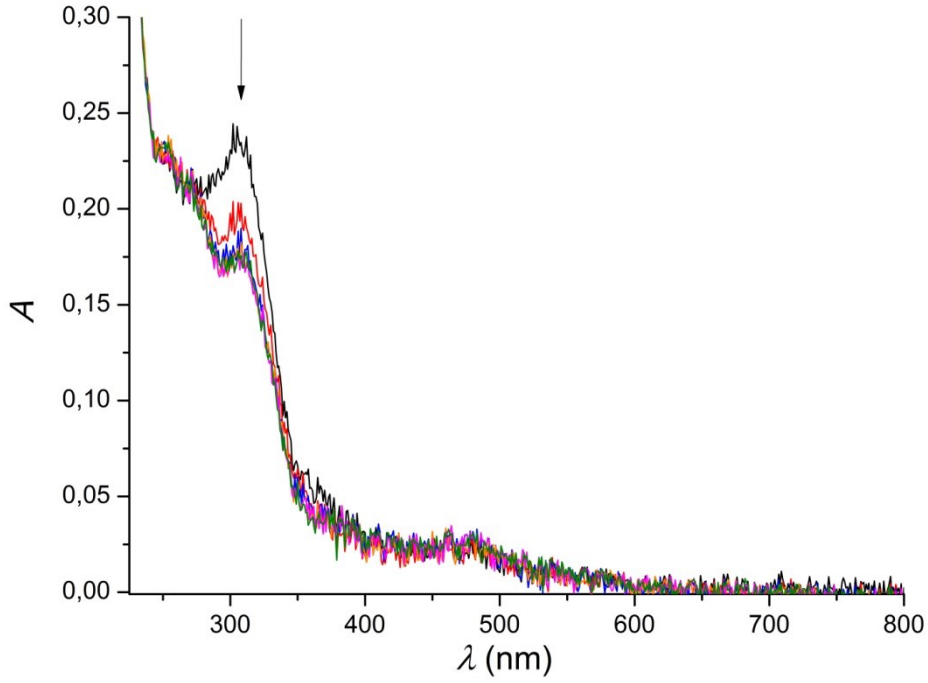
0,30
0,25
0,20
0,15
0,10
0,05
0,00
A
300
400
500
600
700
800
λ (nm)

c)

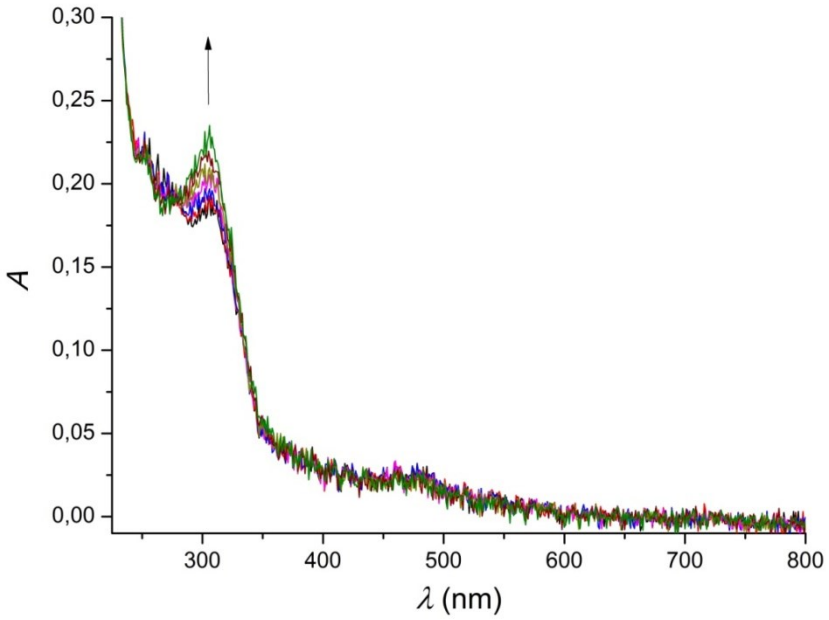

d)

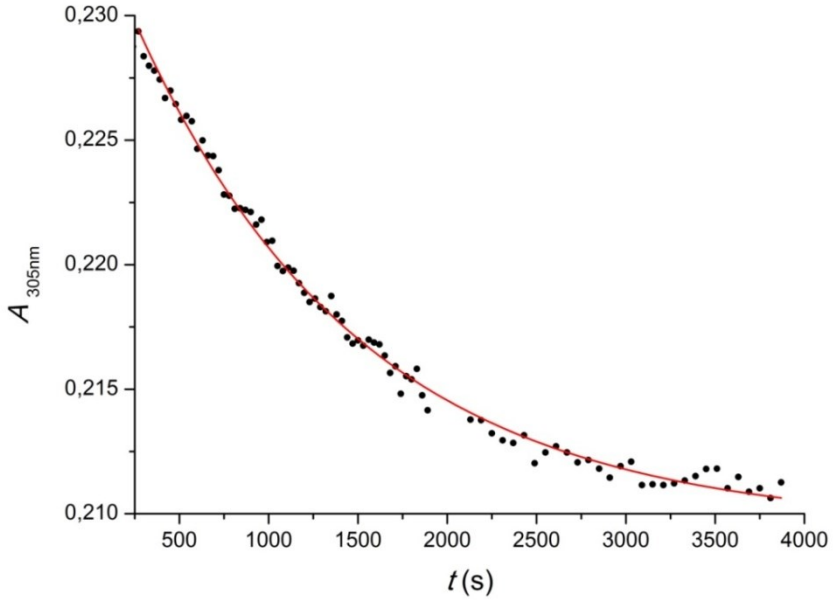

Figure S25. (a): Absorbance at 305 nm vs. time after the addition of 3 equiv of Ce^{IV} to $[Ru(tptzH)(dcb)(OH_2)]^{3+}$, C =1.06x10^{-5} M in $HClO_4$ 0.1 M. **(b)** UV-visible spectra until 45 s. **(c)** UV-visible spectra from 45 s to 5 min; Δt = 9 s. **(d)** Absorbance at 305 nm vs. time in the time range from 250 to 4000 s; experimental values (black dots) and fitting with exponential function of first order (red line).

a)

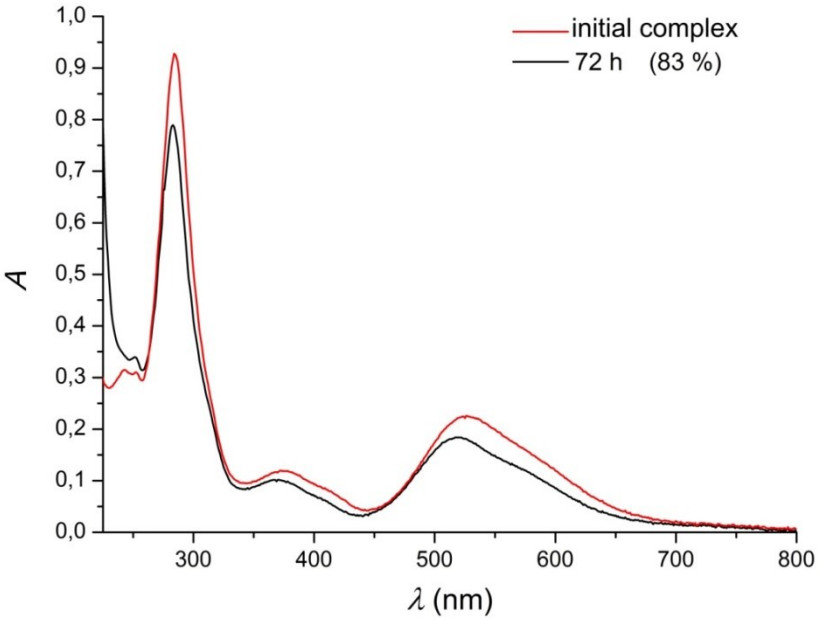
initial complex
72 h (83 %)
A
λ (nm)
1,0
0,9
0,8
0,7
0,6
0,5
0,4
0,3
0,2
0,1
0,0
300
400
500
600
700
800

b)

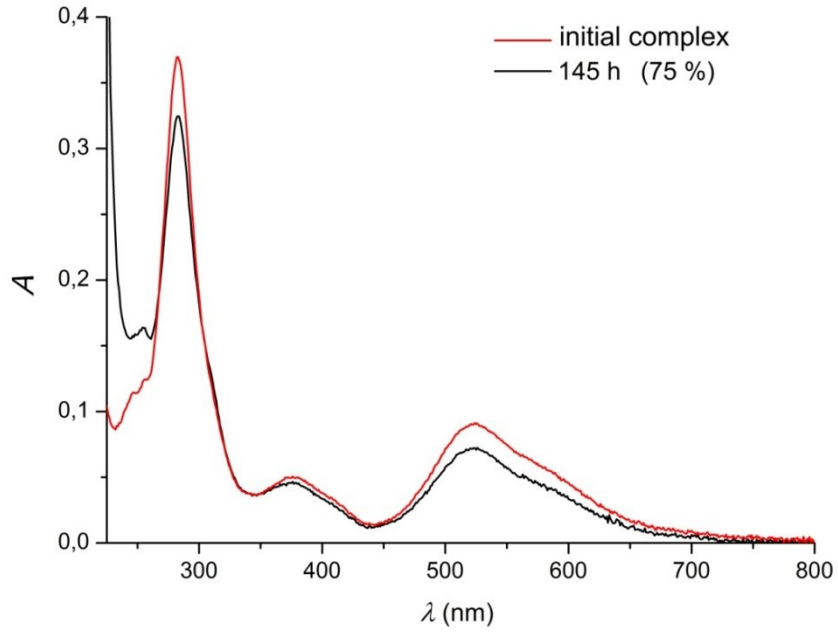
initial complex
145 h (75 %)
A
λ (nm)
0,4
0,3
0,2
0,1
0,0
300
400
500
600
700
800

c)

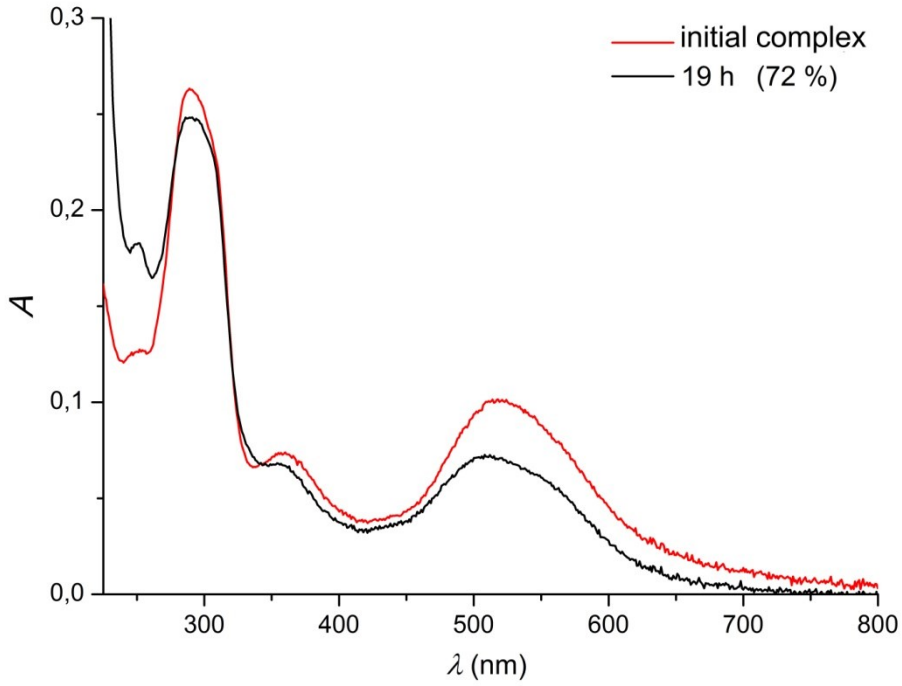

Figure S26. UV-visible spectra initial (red) and final (black) after the reaction with 3 equiv of Ce^{IV} in $HClO_4$ 0.1 M. **(a)** $[Ru(tptzH)(bpy)(OH_2)]^{3+}$,C = $1.6x10^{-5}$ M. **(b)** $[Ru(tptzH)(dmb)(OH_2)]^{3+}$, C =$1.06x10^{-5}$ M. **(c)** $[Ru(tptzH)(dcb)(OH_2)]^{3+}$, C = $1.06x10^{-5}$M.

a)

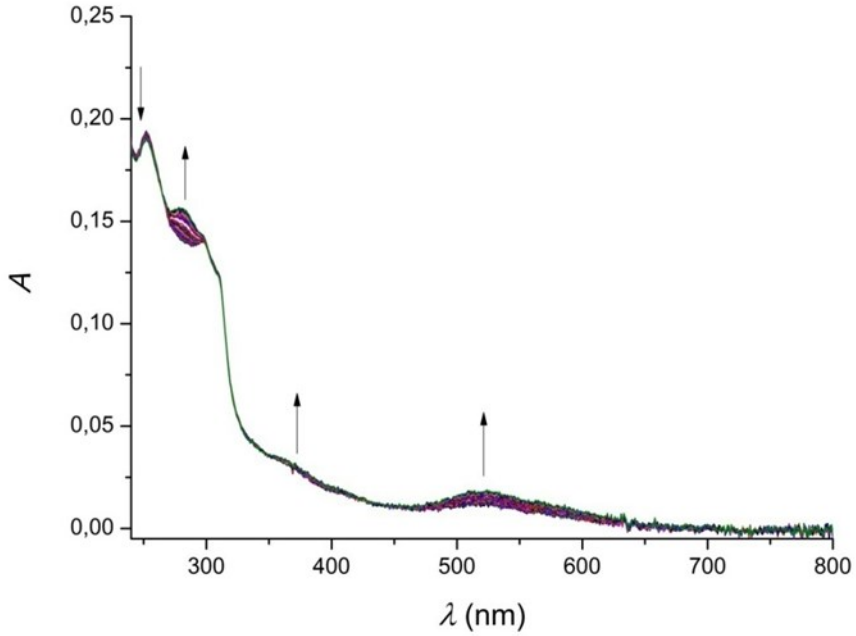

b)

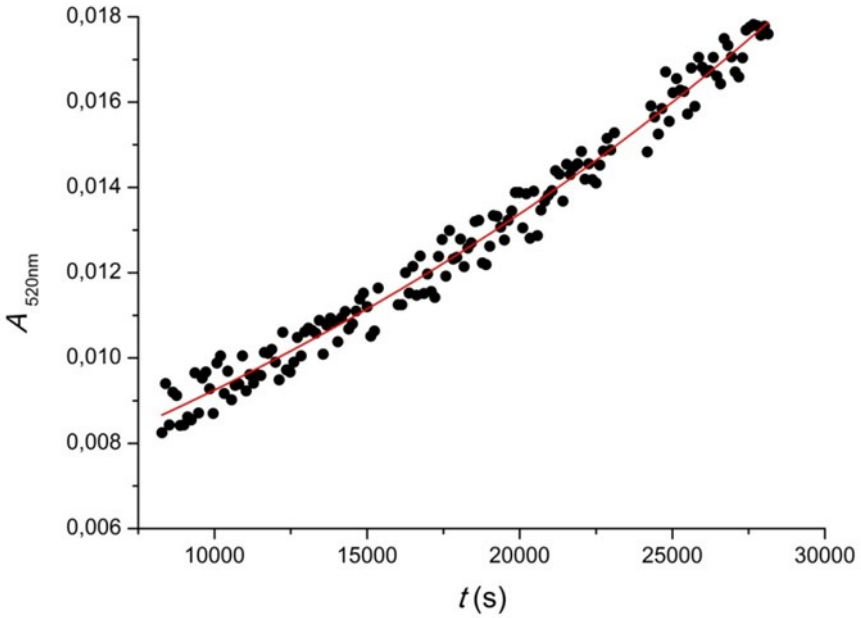

Figure S27.(a): UV-visible spectra for the final of the reaction of $[Ru(tptzH)(dmb)(OH_2)]^{3+}$,C =1.06x10^{-5} M with 4 equiv de Ce(IV) in $HClO_4$ 0.1 M, for the time interval between 125 and 460 min. (b) Absorbance at 520 nm vs. time. Experimental values (black dots) and fitting with exponential function of first order (red line).

a)

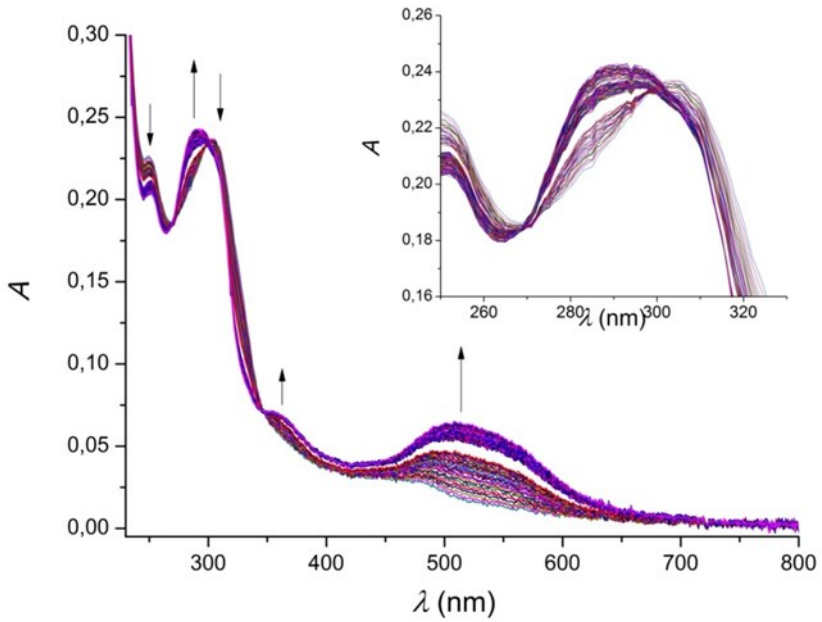

b)

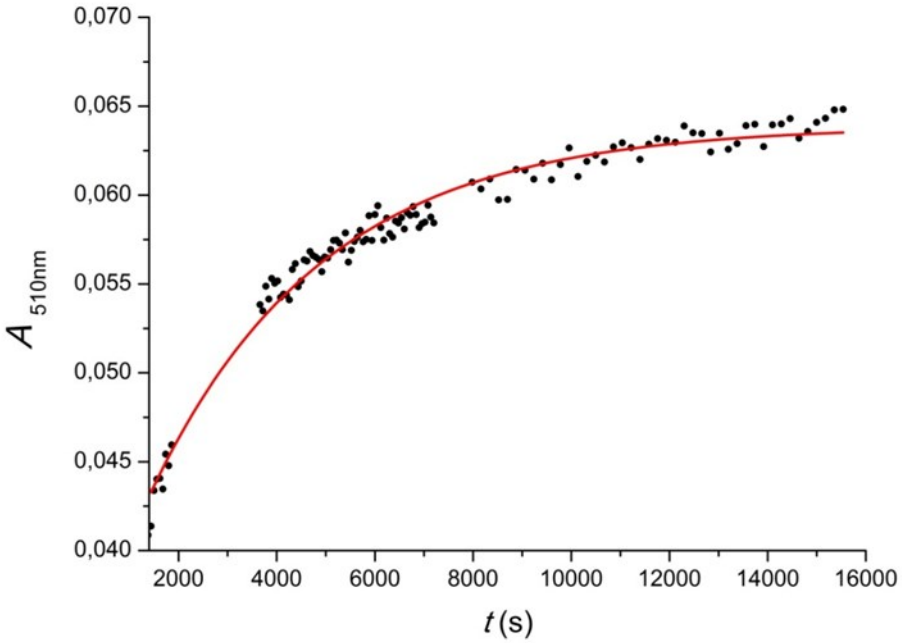

Figure S28.(a): UV-visible spectra for the final of the reaction of $[Ru(tptzH)(dcb)(OH_2)]^{3+}$,C =1.06x10^{-5} M) with 4 equiv de Ce(IV) in $HClO_4$ 0.1 M, for the time interval between 17 and 267 min. Inset: spectra between 240 and 340 nm. (b) Absorbance at 510 nm vs. time. Experimental values (black dots) and fitting with exponential function of first order (red line).

a)

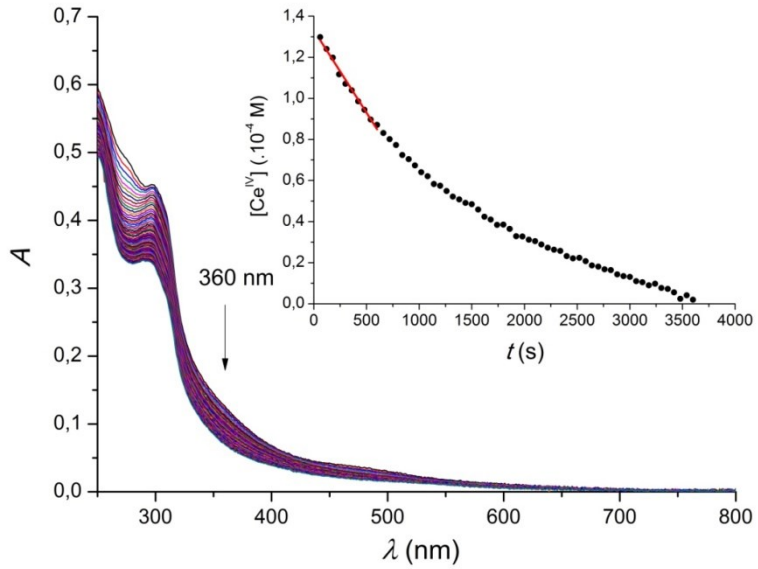

b)

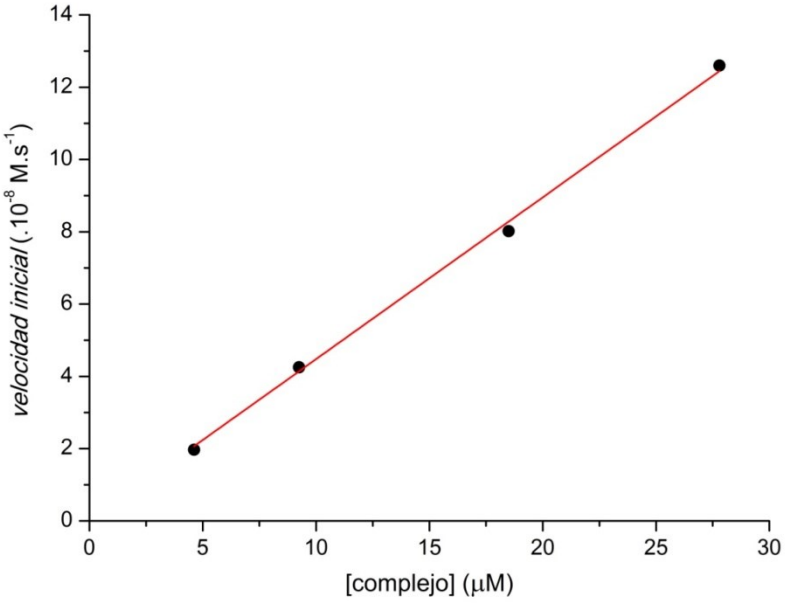

Figure S29. **(a)** UV-visible spectra corresponding to the reaction of $[Ru(tptzH)(dmb)(OH_2)]^{3+}$, C = 1.85x10^{-5} M with Ce^{IV} , C = 2.22x10^{-4} M (12 equiv) in $HClO_4$ 0.1M; Δt = 60 s, t_{total} = 1 h. Inset: [Ce^{IV}] vs. time (black dots) and linear fitting corresponding to intial **rate** (600 s) (red line). (b) Initial rate of Ce^{IV} consumption vs. [complex] in condition of 12 equiv of oxidant (black dots) and linear fitting (red line).

a)

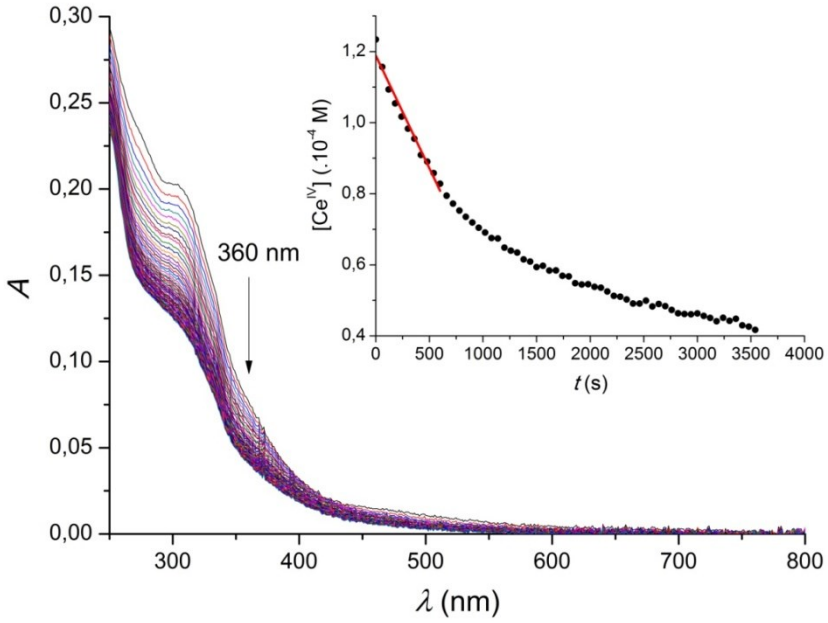

b)

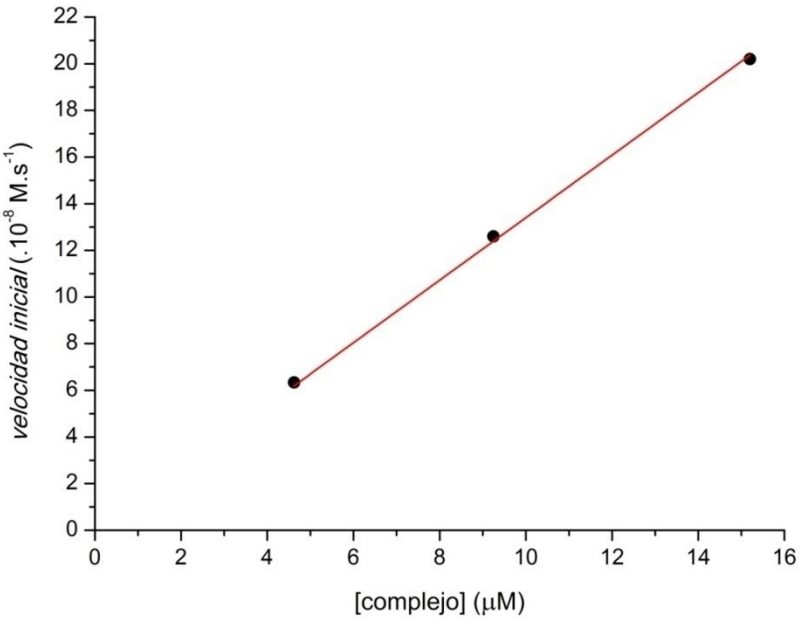

Figure S30. (a) UV-visible spectra corresponding to the reaction of $[Ru(tptzH)(dcb)(OH_2)]^{3+}$, C = 4.62x10^{-6} M with Ce^{IV} , C = 1.39x10^{-4} M (30 equiv) HClO4 0.1M; Δt = 60 s, t_{total} = 1 h. Inset: $[Ce^{IV}]$ vs. time (black dots) and linear fitting corresponding to intial rate (600 s) (red line). **(b)** Initial rate of Ce^{IV} consumption vs. [complex] in condition of 30 equiv of oxidant (black dots) and linear fitting (red line).

a)

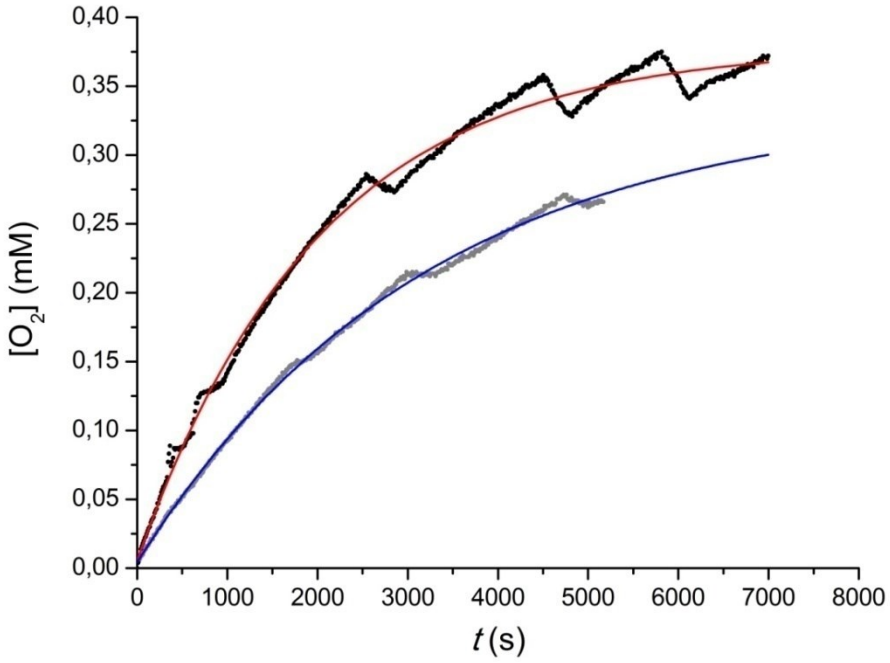

b)

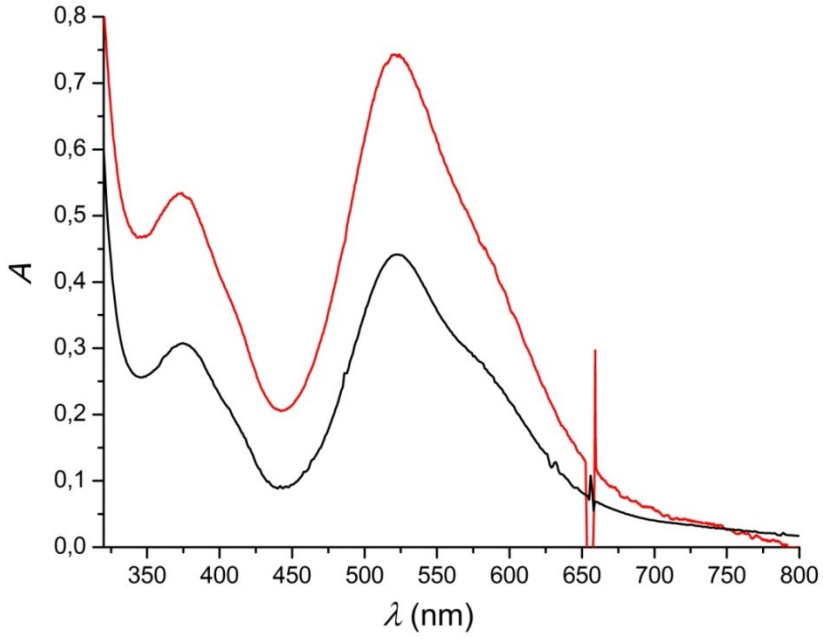

Figure S31. (a) $[O_2]$ vs. time for the reaction of $[Ru(tptzH)(dmb)(OH_2)]^{3+}$, C = $1x10^{-4}$ M) with Ce^{IV}, C= $1.2x10^{-3}$ M (12 equiv) in $HClO_4$ 0.1 M with 9.4 % of acetone (black) and exponential fitting (red); control measurement (gray) and exponential fitting (blue). **(b)** Initial spectra of the complex (red) and final after 2 h (black).

a)

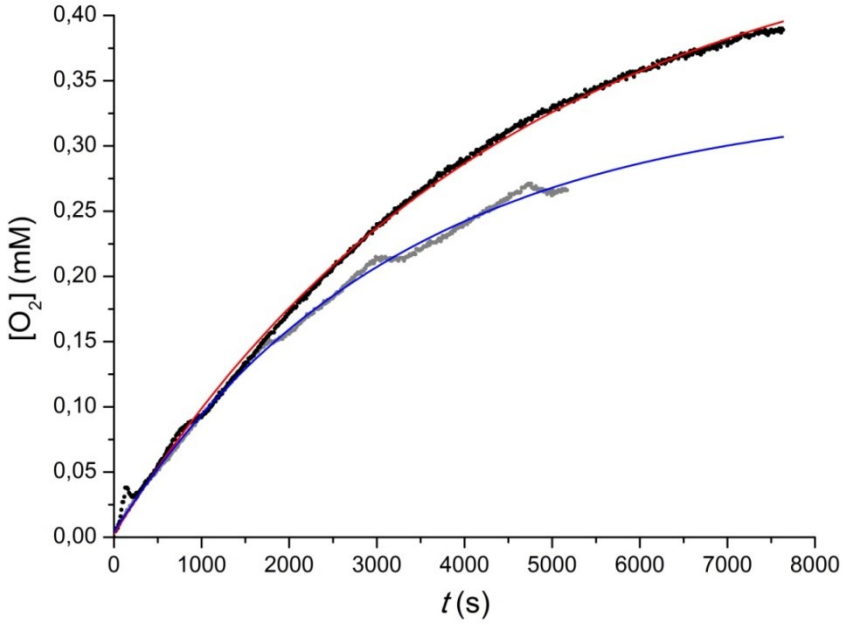

b)

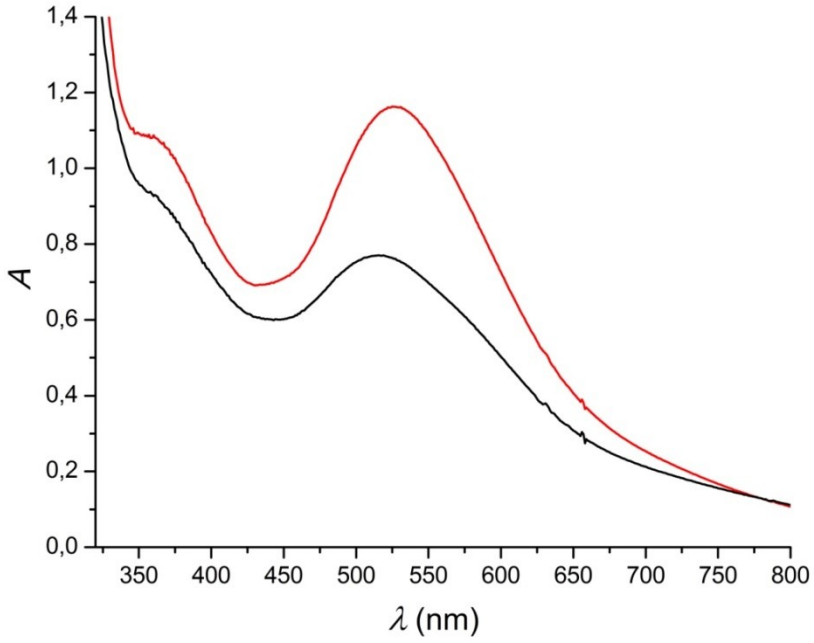

Figure S32. (a) $[O_2]$ vs. time for the reaction of $[Ru(tptzH)(dcb)(OH_2)]^{3+}$, C =1x10^{-4}M with Ce^{IV} , C = 1.2x10^{-3} M (12 equiv) in $HClO_4$ 0.1 M with 9.4 % of acetone (black) and exponential fitting (red); control measurement (gray) and exponential fitting (blue). **(b)** Initial spectra of the complex (red) and final after 2 h (black).

Table S1. Energy (eV) and composition (%) of relevant MO for complex **(4)** and their derivate complexes in different protonation and oxidation states.

Complex	OM	E (eV)	Ru	tptz/tptzH$^+$	bpy	$H_2O/OH^-/O^{2-}$
$[Ru^{II}(tptzH)(bpy)(OH_2)]^{3+}$ $[Ru^{II}\text{-}OH_2]^{3+}$	LUMO+5	-2.01	1	62	37	0
	LUMO+4	-2.41	0	99	0	0
	LUMO+3	-2.8	4	1	95	0
	LUMO+2	-2.91	2	97	0	0
	LUMO+1	-3.72	2	97	0	0
	LUMO	-4.05	9	90	0	0
	HOMO	-6.63	78	12	10	0
	HOMO-1	-6.71	73	14	13	0
	HOMO-2	-6.77	72	22	3	3
	HOMO-3	-7.61	1	0	98	0
	HOMO-4	-8.34	0	100	0	0
	HOMO-5	-8.53	2	98	0	0
$[Ru^{II}(tptz)(bpy)(OH_2)]^{2+}$ $[Ru^{II}\text{-}OH_2]^{2+}$	LUMO+5	-1.68	1	98	2	0
	LUMO+4	-1.91	1	55	44	0
	LUMO+3	-2.24	1	99	0	0
	LUMO+2	-2.71	5	1	95	0
	LUMO+1	-3.35	2	98	0	0
	LUMO	-3.43	9	90	0	0
	HOMO	-6.37	77	12	10	0
	HOMO-1	-6.48	74	14	12	0
	HOMO-2	-6.49	73	21	3	3
	HOMO-3	-7.43	1	99	0	0
	HOMO-4	-7.53	1	1	98	0
	HOMO-5	-7.86	3	96	0	1

$[Ru^{II}(tptz)(bpy)(OH)]^{+}$ $[Ru^{II}\text{-}OH]^{+}$	LUMO+5	-1.47	1	82	16	0
	LUMO+4	-1.69	1	41	58	0
	LUMO+3	-1.98	1	99	0	0
	LUMO+2	-2.46	5	1	94	0
	LUMO+1	-3.01	14	83	1	2
	LUMO	-3.07	4	96	1	0
	HOMO	-5.36	50	18	4	28
	HOMO-1	-5.86	71	18	5	7
	HOMO-2	-6.05	74	12	14	0
	HOMO-3	-7.26	11	35	8	46
	HOMO-4	-7.28	2	91	1	7
	HOMO-5	-7.32	1	2	95	2
$[Ru^{IV}(tptzH)(bpy)(O)]^{3+}$ $[Ru^{IV}\text{-}O]^{3+}$	LUMO+5	-2.7	17	80	2	1
	LUMO+4	-3.02	2	1	97	0
	LUMO+3	-3.17	5	93	1	1
	LUMO+2	-4.04	4	94	0	2
	LUMO+1	-4.34	8	89	1	2
	LUMO	-5.02	43	17	3	37
	HOMO	-6.76	45	11	2	42
	HOMO-1	-7.76	1	0	99	0
	HOMO-2	-8.06	56	16	26	2
	HOMO-3	-8.67	0	98	1	1
	HOMO-4	-8.81	1	88	4	7
	HOMO-5	-8.95	1	91	3	5
$[Ru^{IV}(tptz)(bpy)(O)]^{2+}$ $[Ru^{IV}\text{-}O]^{2+}$	LUMO+5	-2.21	4	85	11	0
	LUMO+4	-2.63	16	81	2	1
	LUMO+3	-2.94	2	1	97	0
	LUMO+2	-3.66	4	94	0	1
	LUMO+1	-3.75	8	89	1	2
	LUMO	-4.76	42	17	3	37
	HOMO	-6.49	46	10	2	42
	HOMO-1	-7.53	4	95	1	0
	HOMO-2	-7.7	2	1	97	0
	HOMO-3	-7.83	43	37	18	2
	HOMO-4	-7.95	8	86	4	2
	HOMO-5	-8.44	0	99	1	1

Table S2. Energy (eV) and composition (%) of relevant MO for complex **(5)** and their derivate complexes in different protonation and oxidation states.

Complex	OM	E (eV)	Ru	tptz/tptzH$^+$	dmb	$H_2O/OH^-/O^{2-}$
$[Ru^{II}(tptzH)(dmb)(OH_2)]^{3+}$ $[Ru^{II}\text{-}OH_2]^{3+}$	LUMO+5	-1.96	2	80	18	0
	LUMO+4	-2.4	0	99	0	0
	LUMO+3	-2.68	3	1	96	0
	LUMO+2	-2.9	2	97	0	0
	LUMO+1	-3.7	2	97	0	0
	LUMO	-4.03	10	89	0	0
	HOMO	-6.55	76	12	13	0
	HOMO-1	-6.62	72	14	14	0
	HOMO-2	-6.72	72	22	3	3
	HOMO-3	-7.53	1	0	98	0
	HOMO-4	-8.32	0	99	1	0
	HOMO-5	-8.48	2	10	88	0
$[Ru^{II}(tptz)(dmb)(H_2O)]^{2+}$ $[Ru^{II}\text{-}OH_2]^{2+}$	LUMO+5	-1.67	0	99	0	0
	LUMO+4	-1.84	2	78	20	0
	LUMO+3	-2.22	1	99	0	0
	LUMO+2	-2.6	4	1	95	0
	LUMO+1	-3.33	2	97	0	0
	LUMO	-3.4	9	90	0	0
	HOMO	-6.28	76	12	12	0
	HOMO-1	-6.39	73	13	13	0
	HOMO-2	-6.43	73	21	3	3
	HOMO-3	-7.42	0	96	3	0
	HOMO-4	-7.45	1	3	96	0
	HOMO-5	-7.85	3	96	0	1
$[Ru^{II}(tptz)(dmb)(OH)]^{+}$ $[Ru^{II}\text{-}OH]^{+}$	LUMO+5	-1.44	1	94	5	0
	LUMO+4	-1.6	2	66	32	0
	LUMO+3	-1.96	1	99	0	0
	LUMO+2	-2.37	4	1	94	0
	LUMO+1	-2.98	16	82	1	2
	LUMO	-3.04	3	96	1	0
	HOMO	-5.32	50	19	4	28
	HOMO-1	-5.81	71	18	5	6
	HOMO-2	-5.97	73	12	15	0
	HOMO-3	-7.23	7	16	44	33
	HOMO-4	-7.25	4	46	33	16
	HOMO-5	-7.26	2	64	27	6
$[Ru^{IV}(tptzH)(dmb)(O)]^{3+}$ $[Ru^{IV}\text{-}O]^{3+}$	LUMO+5	-2.67	14	83	2	1
	LUMO+4	-2.9	2	1	97	0
	LUMO+3	-3.15	4	94	1	1
	LUMO+2	-4.02	4	94	0	2
	LUMO+1	-4.32	9	88	1	2
	LUMO	-4.98	43	17	3	37

	HOMO	-6.71	44	11	2	42
	HOMO-1	-7.68	1	0	98	0
	HOMO-2	-7.9	47	12	40	1
	HOMO-3	-8.54	1	8	89	2
	HOMO-4	-8.67	0	92	7	0
	HOMO-5	-8.78	1	85	6	8

Table S3. Energy (eV) and composition (%) of relevant MO for complex **(6)** and their derivate complexes in different protonation states.

Complex	OM	E (eV)	Ru	tptz/tptzH$^+$	dcb	H_2O/OH^-
$[Ru^{II}(tptzH)(dcb)(OH_2)]^{3+}$	LUMO+5	-2.45	0	99	0	0

$[Ru^{II}\text{-}OH_2]^{3+}$	LUMO+4	-2.85	1	0	98	0
	LUMO+3	-2.96	2	98	0	0
	LUMO+2	-3.42	6	1	93	0
	LUMO+1	-3.79	2	97	1	0
	LUMO	-4.12	9	91	0	0
	HOMO	-6.8	78	13	9	0
	HOMO-1	-6.89	72	14	14	0
	HOMO-2	-6.93	73	21	3	4
	HOMO-3	-7.89	1	0	99	0
	HOMO-4	-8.39	0	100	0	0
	HOMO-5	-8.58	2	98	0	0
$[Ru^{II}(tptz)(dcb)(OH_2)]^{2+}$ $[Ru^{II}\text{-}OH_2]^{2+}$	LUMO+5	-2.29	1	99	0	0
	LUMO+4	-2.37	0	3	96	0
	LUMO+3	-2.8	2	0	98	0
	LUMO+2	-3.34	8	11	81	0
	LUMO+1	-3.43	1	88	11	0
	LUMO	-3.51	8	91	0	0
	HOMO	-6.57	76	13	11	0
	HOMO-1	-6.67	73	22	3	3
	HOMO-2	-6.69	72	14	14	0
	HOMO-3	-7.46	1	99	0	0
	HOMO-4	-7.82	1	1	99	0
	HOMO-5	-7.9	4	95	0	1
$[Ru^{II}(tptz)(dcb^{2-})(OH)]^{-}$ $[Ru^{II}\text{-}OH]^{-}$	LUMO+5	-1.48	2	4	94	0
	LUMO+4	-1.6	1	42	57	0
	LUMO+3	-1.94	1	99	0	0
	LUMO+2	-2.33	5	1	94	0
	LUMO+1	-2.93	17	80	1	2
	LUMO	-3.01	4	96	0	0
	HOMO	-5.36	46	25	2	27
	HOMO-1	-5.74	71	15	7	7
	HOMO-2	-5.99	73	12	15	0
	HOMO-3	-6.34	0	0	100	0
	HOMO-4	-6.37	0	0	100	0
	HOMO-5	-6.5	0	0	99	0

Table S4. TD-DFT (B3LYP-LANL2DZ/CPCM-water) calculated wavelengths of relevant low-lying singlet electronic transitions for complex **(4)** and their derivate protonation species.

Complex	λ(nm)	Oscillator strength	Main components (%) assignments	λ_{exp}(nm)
$[Ru^{II}(tptzH)(bpy)(OH_2)]^{3+}$	542	0.0513	H-2→L+1 (94)	574 (sh)

$[Ru^{II}\text{-}OH_2]^{3+}$			MLCT dπ(Ru^{II})→π*($tptzH^+$)	529
	487	0.4144	H-2→LUMO(54) ; H-1→L+1(27) MLCT dπ(Ru^{II})→π*($tptzH^+$)	
	382	0.0561	H-2→L+2 (17); H-1→L+3 (57) MLCT dπ(Ru^{II})→π*(bpy)	410 (sh) 376
$[Ru^{II}(tptz)(bpy)(OH_2)]^{2+}$ $[Ru^{II}\text{-}OH_2]^{2+}$	520	0.0531	H-2→L+1 (95) MLCT dπ(Ru^{II})→π*(tptz)	501
	464	0.3985	H-2→LUMO (55); H-1→L+1(25) MLCT dπ(Ru^{II})→π*(tptz)	
	444	0.0009	H-1→L+2(20) ; HOMO→L+2(75) MLCT dπ(Ru^{II})→π*(bpy)	350
	397	0.0308	H-1→L+2(64) ; HOMO→L+2(12) MLCT dπ(Ru^{II})→π*(bpy)	
$[Ru^{II}(tptz)(bpy)(OH)]^{+}$ $[Ru^{II}\text{-}OH]^{+}$	530	0.2397	H-1→LUMO(41) ; H-1→L+1(19) ; HOMO→L+1(18) MLCT dπ(Ru^{II}) →π*(tptz)	515
	448	0.151	HOMO→L+3(94) MLCT dπ(Ru^{II}).pπ(O)→π*(tptz)	
	426	0.0617	H-2→L+2(72) MLCT dπ(Ru^{II})→π*(bpy)	357
	377	0.0466	HOMO→L+7(71) MLCT dπ(Ru^{II}).pπ(O)→π*(bpy)	
	360	0.0037	H-1→L+4(74) MLCT dπ(Ru^{II})→π*(bpy)	
	337	0.0773	H-1→L+5(65); H-1→L+7(18) MLCT dπ(Ru^{II})→π*(bpy.tptz)	

Table S5 TD-DFT (B3LYP-LANL2DZ/CPCM-water) calculated wavelengths of relevant low-lying singlet electronic transitions for complex (**5**) and their derivate protonation species

Complex	λ(nm)	Oscillator strength	Main components (%) assignments	λ_{exp}(nm)
$[Ru^{II}(tptzH)(dmb)(OH_2)]^{3+}$	549	0.052	H-2→L+1(93) MLCT dπ(Ru^{II})→π*($tptzH^+$)	580 (sh) 524
$[Ru^{II}\text{-}OH_2]^{3+}$	492	0.4408	H-2→LUMO(57); H-1→L+1(27)	

			MLCT dπ(Ru^{II})→π*($tptzH^+$)	
	403	0.0321	H-1→L+2(61);H-1→L+9(20) MLCT dπ(Ru^{II})→π*($tptzH^+$)	
	379	0.0512	H-1→L+3(50) ; H-1→L+9(18) MLCT dπ(Ru^{II})→π*(dmb)	405 (sh) 377
	378	0.0277	H-1→L+2(18); H-1→L+3(20); H-1→L+9 (41) MLCT dπ(Ru^{II})→π*(dmb)	
$[Ru^{II}(tptz)(dmb)(OH_2)]^{2+}$ **$[Ru^{II}\text{-}OH_2]^{2+}$**	529	0.0529	H-2→L+1(95) MLCT dπ(Ru^{II})→π*(tptz)	498
	468	0.4146	H-2→LUMO(60) ; H-1→L+1 (23) MLCT dπ(Ru^{II})→π*(tptz)	
	395	0.0307	H-3→LUMO(25); H-1→L+2 (47); HOMO→L+2 (11) MLCT dπ(Ru^{II})→π*(dmb)	352
	316	0.0454	H-7→L+1 (10) ; HOMO→L+6 (73) MLCT dπ(Ru^{II})→π*(dmb)	
$[Ru^{II}(tptz)(dmb)(OH)]^{+}$ **$[Ru^{II}\text{-}OH]^{+}$**	530	0.2354	H-1→LUMO (30); H-1→L+1(27); HOMO→L+1(19) MLCT dπ(Ru^{II})→π*(tptz)	543
	451	0.1633	HOMO→L+3 (93) MLCT dπ(Ru^{II}).pπ(O)→π*(tptz)	
	422	0.0791	H-2→L+2 (71); HOMO→L+4 (13) MLCT dπ(Ru^{II})→π*(dmb)	425 (sh) 392
	388	0.0653	H-1→L+3 (75); HOMO→L+5(12) MLCT dπ(Ru^{II})→π*(tptz)	

Table S6 TD-DFT (B3LYP-LANL2DZ/CPCM-water) calculated wavelengths of relevant low-lying singlet electronic transitions for complex (6) and their derivate protonation species.

Complex	λ(nm)	Oscillator strength	Main components (%) Assignments	λ_{exp}(nm)
$[Ru^{II}(tptzH)(dcb)(OH_2)]^{3+}$ **$[Ru^{II}\text{-}OH_2]^{3+}$**	548	0.0499	H-2→LUMO(24); H-1→L+1(63); HOMO→L+1(10) MLCT dπ(Ru^{II})→π*($tptzH^+$)	518

	521	0.0527	H-2→L+1(91) MLCT dπ(Ru^{II})→π*($tptzH^{+}$)	
	488	0.2987	H-2→LUMO(28); H-1→L+1(20); H-1→L+2(22) MLCT dπ(Ru^{II})→π*($tptzH^{+}$)	
	366	0.0728	H-1→L+4(54); HOMO→L+4(26) MLCT dπ(Ru^{II})→π*(dcb)	361
	358	0.1183	H-1→L+4(29); HOMO→L+4(47) MLCT dπ(Ru^{II})→π*(dcb)	
$[Ru^{II}(tptz)(dcb)(OH_2)]^{2+}$ **$[Ru^{II}\text{-}OH_2]^{2+}$**	495	0.0513	H-1→L+1(86) MLCT dπ(Ru^{II})→π*(tptz)	496
	475	0.4248	H-2→L+1(38); H-2→L+2(26); H-1→LUMO(25) MLCT dπ(Ru^{II})→π*(tptz)	
	431	0.0874	H-2→L+2(32); H-1→LUMO(23); HOMO→L+3(25) MLCT dπ(Ru^{II})→π*(dcb)	349
	385	0.083	H-2→L+3(53); HOMO→L+3(38) MLCT dπ(Ru^{II})→π*(dcb)	
	370	0.1052	H-2→L+2(10); H-2→L+3(39); HOMO→L+3(29) MLCT dπ(Ru^{II})→π*(dcb)	
$[Ru^{II}(tptz)(dcb^{2-})(OH)]^{-}$ **$[Ru^{II}\text{-}OH]^{-}$**	693	0.0493	H-1→LUMO(25); H-1→L+1(40); HOMO→L+1(23) MLCT dπ(Ru^{II})→π*(tptz)	518
	541	0.2512	H-1→LUMO(41); HOMO→L+1(38) MLCT dπ(Ru^{II})→π*(tptz)	
	441	0.1713	HOMO→L+3(95) MLCT dπ(Ru^{II})→π*(tptz)	
	411	0.0969	H-2→L+2(79) MLCT dπ(Ru^{II})→π*(dcb^{2-})	362
	403	0.0048	HOMO→L+4(89) MLCT dπ(Ru^{II})→π*(dcb^{2-})	